Thermal fluctuations for a three-beads swimmer

R. Ferretta,[1,2] R. Di Leonardo,[1,3] and A. Puglisi[1,2,4]
[1]*Department of Physics, University of Rome Sapienza, P.le Aldo Moro 2, 00185, Rome, Italy*
[2]*Institute for Complex Systems - CNR, P.le Aldo Moro 2, 00185, Rome, Italy*
[3]*Nanotec - CNR, P.le Aldo Moro 2, 00185, Rome, Italy*
[4]*INFN, University of Rome Tor Vergata, Via della Ricerca Scientifica 1, 00133, Rome, Italy*

(Received 22 November 2023; accepted 20 May 2024; published 29 July 2024)

We discuss a microswimmer model made of three spheres actuated by an internal active time-periodic force, tied by an elastic potential, and submitted to hydrodynamic interactions with thermal noise. The dynamical approach we use, replacing the more common kinematic one, shows the instability of the original model and the need of a confining potential to prevent the evaporation of the swimmer. We investigate the effect of the main parameters of the model, such as the frequency and phase difference of the periodic active force, the stiffness of the confining potential, the length of the swimmer and the temperature and viscosity of the fluid. Our observables of interest are the averages of the swim velocity, the energy consumption rate, the diffusion coefficient, and the swimming precision, which is limited by the energy consumption through the celebrated thermodynamic uncertainty relations. An optimum for velocity and precision is found for an intermediate frequency. Reducing the potential stiffness, the viscosity, or the length is also beneficial for the swimming performance, but these parameters are limited by the consistency of the model. Analytical approximation for many of the relevant observables is obtained for small deformations of the swimmer. We also discuss the efficiency of the swimmer in terms of its maximum precision and of the hydrodynamic, or Lighthill, criterion, and how they are connected.

DOI: 10.1103/PhysRevResearch.6.033117

I. INTRODUCTION

The physics of active particles is a prominent application of nonequilibrium statistical mechanics [1,2]. Several interesting challenges in this field belong to the category of collective phenomena and emergent order, such as motility-induced phase separation and flocking, which are usually investigated theoretically through simplified models where each particle has no internal structure but only a "self-propulsion" force with simple properties [3–5]. However, a fascinating aspect of the physics of active systems is the mechanism of self-propulsion itself [6]. Self-propulsion typically originates from complex mechanisms and—even when considering microscopic systems—may be based upon the conspiracy of a number of subunits, such as molecular motors [7]. For this reason, in some cases, statistical physics becomes useful also for understanding what happens in a single self-propelling unit [8,9].

Swimming at the micro scale requires strategies to break time-reversal invariance in the absence of relevant inertia, i.e., circumventing the "scallop" theorem [10,11]. A simple mechanism is to perform a periodic nonreciprocal change of shape: the swimmer exploits some source of energy in order to make internal changes and explore a sequence of configurations which is periodic without being time symmetric, the minimal example being $A \to B \to C \to A$. This sequence becomes a limit cycle in the case of a system whose shape is characterized by continuous parameters. Biological systems offer a plethora of examples for such a behavior, the most common instances being self-propelling cells equipped with pushing or pulling flagella or cilia, e.g., motile cells, sperms, bacteria, and *C. reinhardtii* algae [12]. The sperm tail, for instance, excited by a myriad of molecular motors innervating the axoneme, and under the constraints of elasticity and hydrodynamics, displays a wave deformation continuously traveling from the head to the end tip that pushes forward the cell [8]. More simple models have been introduced in the literature, in order to pinpoint the essential mechanism behind the strategies invented by nature and potentially useful for the design of artificial swimming micromachines. Historically, the ancestor of simplified, analytically treatable models is the Lighthill squirmer [13]. A more recent model is the so-called three-beads swimmer, whose analytical treatment is even more manageable, at least in some limits [14,15]. This model, which has also been realized experimentally, has been rarely studied in the presence of noise; see, for instance, Refs. [16–19]. Noise is not only a realistic and interesting perturbation to be added to the limit cycle of a microswimmer, but may offer a new test ground for the so-called thermodynamic uncertainty relations (TUR) which establish a bound to the signal-to-noise ratio based upon the energy consumption of the system [20,21].

Here, we analyze the behavior of the three-beads swimmer when it feels the effect of thermal noise. For the purpose of this study we modified the original three-beads swimmer model in order to be described dynamically instead of kinematically. The result of this change of perspective shows a

crucial problem of the original system, i.e., the lack of stability of its limit cycle. To solve this problem we have introduced an additional elastic force keeping together the three beads and avoiding the observed instability. We underline that noise for a real or model microswimmer may have two distinct origins: thermal noise originated in the molecular agitation of the surrounding fluid or of the swimmer's body, and active noise originated in the randomness of the dynamics of the subunits, such as molecular motors, actuating the swimmer. It is clear that, ultimately, active noise can be traced back to thermal noise, but in a mesoscopic model it would be distinct from it and, for the purpose of the present study, it is ignored. After introducing the model and showing the results of its numerical solutions, we also pose the question of efficiency in terms of different definitions, one being the distance from the bound dictated by the TUR. We show that spatial correlations in the noise due to hydrodynamic interactions (originated in the fluid momentum conservation) modify such an efficiency, a fact which is usually neglected in models of engines or swimmers constituted by several coupled motors [8,22–27]. The consequences also for other figure of merits, such as the Lighthill efficiency, are discussed.

Here, we briefly review the existing literature that is relevant for our study. Concerning the requirement of a binding force keeping the beads close, we recall that the original paper introducing the three-spheres model [14] already considers an implicit link between the beads, however it is not explicitly, i.e., dynamically, modeled. Up to our knowledge, papers that precede our introduction of harmonic binding forces and the corresponding linear approximation for the prediction of the average velocity of the swimmer are Refs. [28,29]; however, they do not discuss the two main points of our study: (1) the lack of stability in the case where there are no binding forces, and (2) the effect of fluctuations and the thermodynamic bounds for the precision rate. Another paper with analogous results, with no discussion of the two aforementioned points, is Ref. [30], but for a slightly different model where one rod (connecting spheres 1 and 2) is kinematically forced while the other one (connecting spheres 2 and 3) is a harmonic spring without force. Reference [31] is an interesting experiment where the three spheres are linked by capillary forces (menisci) due to the air-water interface deformation, while a model with harmonic linking forces well reproduces the results; however, (again) no mention is made of the problem of instability of nonlinked models or of the thermal fluctuations. Finally, Ref. [17] is quite a faithful experimental realization of the original model [14], where optical tweezers dictate the relative position of the beads (with each bead harmonically attached by the optical force to the dictated position).

A discussion of the effect of stochastic active forces on the three-beads swimmer model can be found in Ref. [18]. A more recent paper about the stochastic thermodynamics of the same model is Ref. [19]. The theory of fluctuations for flagellar microswimmers, induced by stochastic dynamics of the molecular motors actuating them, has been investigated in sophisticated [32] and simpler models [33]. Experiments on these fluctuations have been performed in Refs. [8,34].

The structure of the paper is the following. In Sec. II we describe the model, briefly review previous studies concerning it, explain the differences between a kinematic and dynamic approach, introduce the properties of hydrodynamic thermal noise, and finally describe in detail the observables of interest. In Sec. III we report the results of the numerical simulations. In Sec. IV we discuss the thermodynamic uncertainty relation and the Lighthill efficiency. In Sec. V we discuss analytical results in the linearized limit for the velocity of the swimmer and sketch some approximate formula for its diffusivity and noise-to-signal ratio. Finally, in Sec. VI we draw conclusions and discuss perspectives.

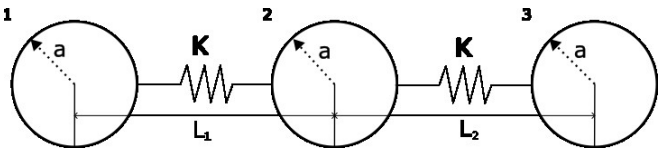

FIG. 1. Sketch of the swimmer model made of three spheres of radius a, distances L_1 and L_2, and springs with stiffness K.

II. THE MODEL

The three-beads model we consider here, see the sketch in Fig. 1, is represented by the equations of motion for three spherical particles (index $i = 1, 2, 3$) of radius a immersed in a fluid of viscosity η, with no rotation or internal degrees of freedom; each particle i is described by velocity vector $\mathbf{v}_i$ and submitted to internal force vector $\mathbf{f}_i$ and external noise vector $\mathbf{f}_i^R$. The condition that the force vector is internal reads $\sum_i \mathbf{f}_i = 0$. The system, in the Stokesian regime (high viscosity, negligible inertia), is described by the instantaneous balance between viscous drags and applied forces, which can be written in the usual form:

$$\mathbf{v}_i = \sum_j H_{ij}(\mathbf{r}_i - \mathbf{r}_j)\big(\mathbf{f}_j + \mathbf{f}_j^R\big). \tag{1}$$

Here, $H_{ij}(\mathbf{r}) = \frac{1}{6\pi\eta a}[\delta_{ij} + (1-\delta_{ij})\frac{3a}{4r}(\mathbb{1} + \hat{\mathbf{r}}\hat{\mathbf{r}})]$ is the Oseen mobility tensor which comes from the solution of the Stokes equation. We recall that the Oseen tensor describes the part of the sphere-sphere hydrodynamic interaction that decreases inversely as the first power of the distance between the spheres and becomes inaccurate at short ranges [35].

The three beads are allowed to move only along one direction—say, $\hat{x}$—and all the forces act only along that direction. This is, of course, not realistic in the case of thermal noise, but we adopted such an assumption in order to keep the problem simple. Assuming that this constraint does not affect the validity of Eq. (1), the x_i coordinates obey the following relation between velocities and forces:

$$\frac{dx_i(t)}{dt} = \sum_j T_{ij}(\underline{x})\big[F_j(\underline{x}, t) + F_j^R(\underline{x}, t)\big], \tag{2}$$

where T_{ij} represents the mobility coefficient coupling the x component of the force acting on particle j and the x component of the velocity of the particle i, while the F_j represent the x components of the forces $\mathbf{f}_j$. We use $\underline{x}$ and $\underline{F}$ to represent the 3-ple $\{x_1, x_2, x_3\}$ and $\{F_1, F_2, F_3\}$. From the Oseen tensor, the matrix $\mathbf{T}$ is obtained by the relation $T_{ij}(\underline{x}) = H_{ij}(\mathbf{r}_i -$

$\mathbf{r}_j)_{xx}$. Therefore, it takes the form

$$\mathbf{T} = \begin{pmatrix} \frac{1}{6\pi\eta a} & \frac{1}{4\pi\eta L_1} & \frac{1}{4\pi\eta(L_1+L_2)} \\ \frac{1}{4\pi\eta L_1} & \frac{1}{6\pi\eta a} & \frac{1}{4\pi\eta L_2} \\ \frac{1}{4\pi\eta(L_1+L_2)} & \frac{1}{4\pi\eta L_2} & \frac{1}{6\pi\eta a} \end{pmatrix}, \tag{3}$$

where $L_1 = x_2 - x_1$ and $L_2 = x_3 - x_2$.

The deterministic forces $\underline{F}$ are the sum of internal conservative (a confining potential to avoid instabilities) and internal nonconservative forces (a time-dependent periodic perturbation that conserves total momentum, also denoted as "active force"), i.e., $\underline{F} = \underline{F}^{\rm act} + \underline{F}^{\rm pot}$, all detailed below. All symbols are introduced in the text, however a list of all relevant symbols is present in Appendix B, Table I.

A. Original setup

The original three-beads model was described by the same equations in (2), without noise i.e., $F_j^R \equiv 0$, and with $F_j(\underline{x}, t)$ reduced to only internal nonconservative forces: $F_j(\underline{x}, t) = F_j^{\rm act}(t)$ with

$$F_1^{\rm act}(t) + F_2^{\rm act}(t) + F_3^{\rm act}(t) = 0. \tag{4}$$

The instantaneous velocity of the center of mass $V = \frac{1}{3}(v_1 + v_2 + v_3)$ was computed in the limit of small deformation of the swimmer, i.e., by assuming

$$L_1 = l_1 + u_1, \quad L_2 = l_2 + u_2, \tag{5}$$

where l_1 and l_2 are constant while u_1 and u_2 are time dependent: for small u_1, u_2 the following formula was obtained:

$$v = \overline{V} = \frac{\alpha}{2}\overline{(u_1\dot{u}_2 - u_2\dot{u}_1)}, \tag{6}$$

with

$$\alpha = \frac{a}{3}\left[\frac{1}{l_1^2} + \frac{1}{l_2^2} - \frac{1}{(l_1+l_2)^2}\right]. \tag{7}$$

For instance, when $u_{1,2}$ obey the oscillation laws

$$\begin{aligned} u_1(t) &= d_1 \cos(\omega t + \phi_1), \\ u_2(t) &= d_2 \cos(\omega t + \phi_2), \end{aligned} \tag{8}$$

one has that the average swimming velocity reads

$$v = \overline{V} = \frac{\alpha}{2} d_1 d_2 \omega \sin(\phi_1 - \phi_2). \tag{9}$$

It is important to realize that the above formulas are based upon the knowledge of $u_i(t)$ and not from the knowledge of the forces $F_i(t)$. This is what we call a kinematic approach and implies that the distances among the particles are prescribed by definition. In the rest of the paper we change the point of view and start from the knowledge of the forces.

B. Difference between kinematic and dynamical approach: Instability of the relative distances

In the rest of the paper we adopt a dynamic point of view, i.e., we set the forces acting on the first and third particles:

$$F_i^{\rm act}(t) = F_0 \cos(\omega t + \phi_i), \quad i = 1, 3, \tag{10}$$

with the constraint in Eq. (4). The reason for this different approach is that when out of equilibrium, i.e., under the presence of nonconservative forces, the properties of the fluctuations of the relative positions of the particles—due to interaction with the molecules of the fluid—are not known in general. On the contrary, one may reasonably describe the effects of these interactions in terms of known fluctuating forces, which is exactly what we call F_i^R; see later for explicit formula. In the whole paper we set $\phi_1 = \Delta\phi$ and $\phi_3 = 0$ [the force $F_2(t)$ is entirely deduced by the knowledge of F_1 and F_3 through the force constraint of internal forces, Eq. (4)].

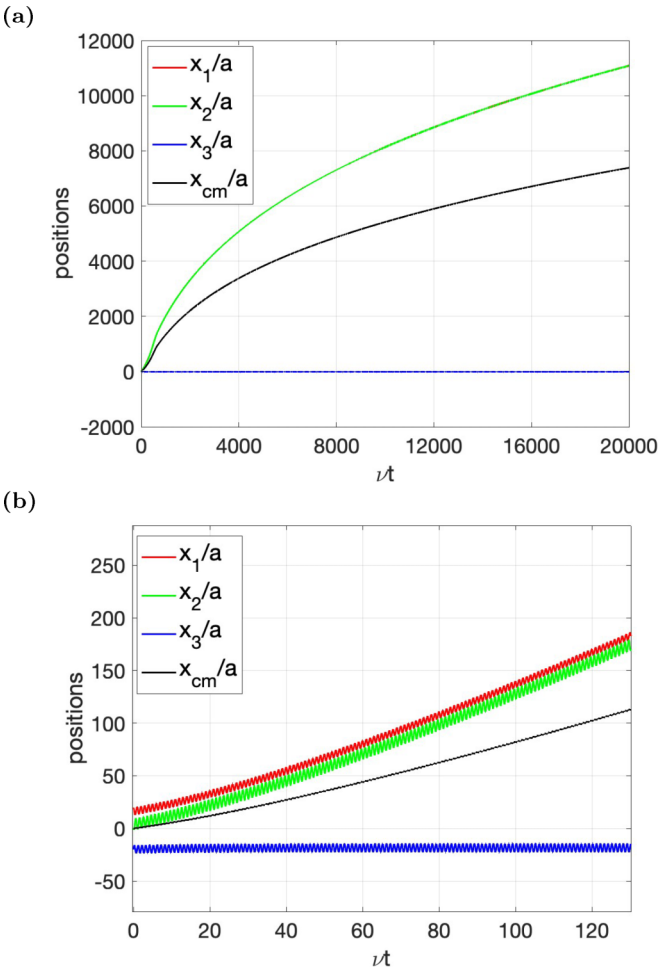

FIG. 2. Positions of the three spheres when there is no noise and no elastic potential. Initial arms length $x_2(0) - x_1(0) = x_3(0) - x_2(0) = 20$, spheres' radius $a = 1$, $\eta = 1$, $\Delta\phi = \pi/2$, $\omega = 2\pi/50$, $F_0 = 10$. (a) Full duration of the simulation, and (b) zoom on early times.

Remarkably, when changing the point of view from kinematic to dynamic, it is possible to show a weakness of the original model, i.e., an intrinsic instability toward the evaporation of the swimmer: the particles' relative distances do not remain limited and the velocity of the swimmer, for this reason, tends to vanish. An example of the numerical solution of the model in Eq. (2) with zero temperature ($F^R = 0$) and $F_i = F_i^{\rm act}(t)$ expressed by Eq. (10) is shown in Fig. 2.

In the figure it is seen that particles 1 and 2 remain close to each other and very far from particle 3. The latter only feels force F_3 with time-average zero. The formers, on the contrary, feel the forces F_1 and F_2 (whose sum is never 0)

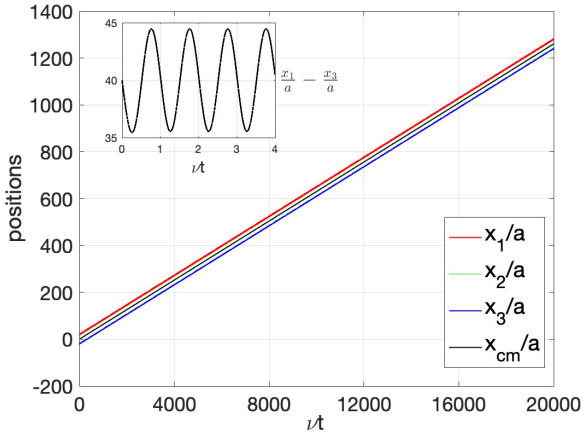

FIG. 3. Positions of the three spheres with the elastic potential and without noise. Parameters: $l_1 = l_2 = L = 20$, $a = 1$, $\eta = 1$, $\Delta\phi = \pi/2$, $\omega = 2\pi/50$, $K = 2$, $F_0 = 10$. The inset shows the distance among particles 1 and 3 for a small number of perturbation periods.

which have zero time average, but they also feel the hydrodynamic interactions which depend upon the relative distance: a closer inspection (not shown) reveals that the distance between particles 1 and 2 oscillates modulating the pair mobility to be in phase with total force $F_1 + F_2$ acting on the pair. As a consequence, even if $F_1 + F_2 = 0$ on average, the mean speed is different from zero. However, the excursion of the couple's distance very slowly decreases in time, leading to a reduction of the effective force and therefore velocity. A fit of the position of particles 1 and 2 in time suggests that $x_1 \sim x_2 \sim t^{1/3}$ and therefore a vanishing velocity is expected at large times. In Sec. V we discuss the linear stability of the limit cycle (in the plane L_1, L_2), showing the presence of a positive eigenvalue for all the values of the oscillating forces, which explain the initial instability of the three-beads state.

For this reason we introduce a harmonic attractive potential among each couple of adjacent spheres, i.e.,

$$\underline{F}(\underline{x}, t) = \underline{F}^{\text{act}}(t) + \underline{F}^{\text{pot}}(\underline{x}) \tag{11}$$

with

$$F_1^{\text{pot}} = K(x_2 - x_1 - l_1) \tag{12}$$

$$F_2^{\text{pot}} = K(x_3 - x_2 - l_2) - K(x_2 - x_1 - l_1) \tag{13}$$

$$F_3^{\text{pot}} = -K(x_3 - x_2 - l_2), \tag{14}$$

with K the elastic constant and l_1, l_2 the lengths at rest of the harmonic springs. When $K > 0$ we observe that the instability disappears and the relative positions of the three spheres remain limited, see Fig. 3.

It is interesting to note that an experimental realization of the three-beads swimmer has been obtained by applying a time-modulated magnetic field on permanently magnetized spheres *linked* by elastic rods [36]. Physical links, however, are not the only possibility for experimental implementations; see, for instance Ref. [17]. A theoretical study of a swimming system of beads with the presence of elastic confining potential can be found in Ref. [37] by prescribing a cyclical law for the length at rest of the potentials, l_1, l_2, and ignoring the effect of thermal noise as well as energetic considerations. In the rest of the paper we assume that the lengths at rest are equal ("symmetric swimmer") $l_1 = l_2 = L$, but in the Appendix we consider the most general case $l_1 \neq l_2$.

C. Details of the noise

A passive colloidal particle moves under the stochastic effect of the molecules of the surrounding fluid, i.e., what is called thermal noise and is described by the physics of Brownian motion [38]. When more colloidal particles are present, spatial correlations appear in the thermal forces acting on each particle [39]. The simplest explanation for such correlations is the consistency between noise and dissipation dictated by the fluctuation-dissipation relation of the second kind, which generalizes the Einstein relation between mobility and diffusivity: since dissipation appears as a matrix of correlated mobilities (the Oseen tensor), also noise must be described by a matrix of correlated diffusivities [40,41]. The physical counterpart of this consistency argument is the fact that an incompressible viscous fluid transmits forces acting in a point over a long distance, and this principle holds for both dissipative and fluctuating forces [42].

The fluctuation dissipation relation of the second kind, which relates the diffusivity matrix $\mathbf{D}$ and the mobility matrix $\mathbf{T}$ in our terms, reads $\mathbf{D} = \mathbf{T}/\beta$, where $\beta = 1/(k_B T)$ is the inverse temperature (in the simulations we assume unitary Boltzmann constant $k_B = 1$) [40]. Since $\mathbf{T}$ depends upon the coordinates $\underline{x}$, the Fokker-Planck equation for the process is not uniquely determined by D. The ambiguity is removed, asking for detailed balance (i.e., absence of physical currents) when the nonconservative forces are absent. Then, following, for instance, Ref. [43], this condition implies the following form for the probability current:

$$J_i(\underline{x}, t) = \sum_j D_{ij}[\beta F_j(\underline{x}, t) P(\underline{x}, t) - \partial_{x_j} P(\underline{x}, t)], \tag{15}$$

appearing in the Fokker-Planck equation

$$\partial_t P(\underline{x}, t) = -\partial_{x_i} J_i(\underline{x}, t). \tag{16}$$

Such a Fokker-Planck equation implies the following anti-Ito stochastic differential equation to hold:

$$dx_i = \sum_j [T_{ij} F_j]\, dt + \sqrt{\frac{2}{\beta}} \sum_j T_{ij} [\sqrt{\zeta} \cdot d\mathbf{W}(t)]_j, \tag{17}$$

or conversely, the following Ito stochastic differential equation:

$$dx_i = \sum_j \left[T_{ij} F_j + \frac{1}{\beta} \partial_{x_j} T_{ij} \right] dt + \sqrt{\frac{2}{\beta}} \sum_j T_{ij} [\sqrt{\zeta} \cdot d\mathbf{W}(t)]_j, \tag{18}$$

which is better suited for numerical integration and theoretical calculations. Three additional terms appear, which we call "Ito forces" (they are actually velocities) defined as $F_{\text{Ito},i} =$

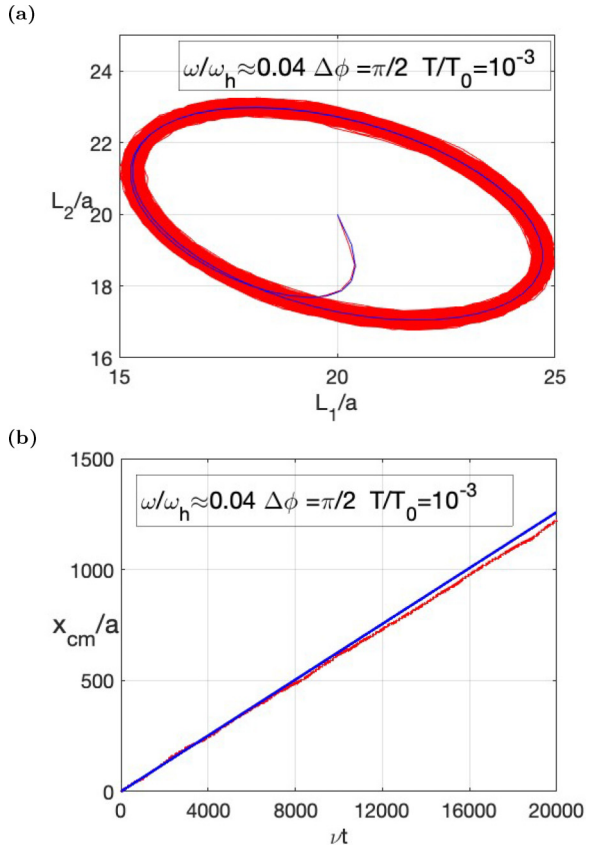

FIG. 4. (a) Arms' length in comparison, with (red) and without noise (blue). (b) Position of the center of mass with (red) and without noise (blue). Parameters: $L = 20$, $a = 1$, $\eta = 1$, $\Delta\phi = \pi/2$, $\omega = 2\pi/50$, $K = 2$, $F_0 = 10$, (blue) $T = 0$, and (red) $T = 0.01$.

$\frac{1}{\beta}\sum_j \partial_{x_j} T_{ij}$, that read

$$F_{\text{Ito},1} = \frac{1}{\beta}\frac{\frac{1}{L_1^2} + \frac{1}{(L_1+L_2)^2}}{4\pi\eta}, \tag{19}$$

$$F_{\text{Ito},2} = \frac{1}{\beta}\frac{(L_1 - L_2)(L_1 + L_2)}{4\pi\eta L_1^2 L_2^2}, \tag{20}$$

$$F_{\text{Ito},3} = -\frac{1}{\beta}\frac{\frac{1}{L_2^2} + \frac{1}{(L_1+L_2)^2}}{4\pi\eta}. \tag{21}$$

We remark that $\sqrt{\zeta}$ is a matrix such that $\sqrt{\zeta}[\sqrt{\zeta}]^T = \mathbf{T}^{-1}$. For the purpose of numerical integration we adopted the Cholesky decomposition of $\mathbf{T}^{-1}$ as a representation of it.

We conclude this subsection by showing, see Fig. 4, the effect of the noise, at a relatively small temperature (see next subsection for a discussion of the physical meaning of the units we use in the numerical simulations). The figure shows both the trajectory of the center of mass of the swimmer, as well as its trajectory in phase space, i.e., the plot of $L_1(t) = x_2(t) - x_1(t)$ versus $L_2(t) = x_3(t) - x_2(t)$, in the case of both $T = 0$ and $T = 10^{-2}$. As we will discuss later, a clear effect of the growth of temperature (i.e., of noise) is an increase of the diffusivity and therefore of transient deviations from the average trajectory, which become hardly distinguishable when the total time is increased and the average swimming motion dominates.

D. Units of the physical parameters

We give all the results in arbitrary units. Here, we discuss a possible conversion of those units in physical units. The candidate conversion to International System units is

$$1\,\text{space unit} = 10^{-6}\text{m} = 1\,\mu\text{m}, \tag{22}$$

$$1\,\text{time unit} = 10^{-3}\text{s} = 1\,\text{ms}, \tag{23}$$

$$1\,\text{force unit} = 5 \times 10^{-14}\,\text{N}, \tag{24}$$

$$\text{or equivalently,} \tag{25}$$

$$1\,\text{mass unit} = 5 \times 10^{-14}\,\text{kg}. \tag{26}$$

With such a conversion table, we get that $T = 0.1$ in arbitrary units corresponds to $T \approx 300\,\text{K}$, and a viscosity $\eta = 1$ in arbitrary units corresponds to $\eta = 5 \times 10^{-5}\,\text{Pa s}$, which is 20 times smaller than water viscosity. A period of 50, i.e., $\omega = 2\pi/50 \approx 0.12$ in arbitrary units, corresponds to $\omega \approx 20\,\text{Hz}$. A velocity of the center of mass $v = 10^{-3}$ corresponds to $v = 1\,\mu\text{m/s}$.

E. Characteristic values of the parameters

For the numerical study we need to define a few characteristic numbers which can be useful as a reference in the presentation of the results, in order to draw adimensional axes in the graphs. We define $\nu = \omega/2\pi$ as the forcing frequency; $v_0 = \omega a F_0^2/(L^2K^2)$, which is the swimming velocity expected for small forcing amplitudes, and in the adiabatic limit $\omega \to 0$ (see the linear theory in Sec. V); $K_0 = F_0/a$ a typical stiffness related to the forcing amplitude F_0 and the diameter of the spheres a; $\eta_0 = F_0/(6\pi v_0 a) = (KL)^2/(6\pi a^2 F_0 \omega)$ a typical viscosity related to forcing, swimming velocity, and diameter a; note that when $\omega = 2\pi/10$ (i.e., forcing period 10 ms with the units assumed above, one has $\eta_0 \sim 13.5$, which is close to water viscosity in the same units), $T_0 = F_0 * a$ a typical thermal energy (temperature having assumed $k_B = 1$). When we present results as a function of ω, the above choices for characteristic parameters cannot be used, therefore we introduce other characteristic parameters related to hydrodynamics, i.e., $\nu_h = F_0/(6\pi\eta a^2)$ a hydrodynamic frequency (close to 0.5 in most of the other plots) and the corresponding pulsation $\omega_h = 2\pi\nu_h$, and finally an associated swimming velocity $v_h = 2\pi\nu_h a F_0^2/(L^2K^2)$.

F. Observables of interest in the numerical integration

In the rest of the paper we report several observations obtained by numerical integration of Eq. (18) by a simple Euler scheme, i.e., by replacing dt with the time step $\Delta t = 10^{-2}$, replacing each Wiener increment $dW_i(t)$ with a Gaussian-distributed random number (independent from each other) with zero average and variance Δt, and replacing $dx_i(t)$ with $x_i(t + \Delta t) - x_i(t)$. We have verified that reducing further the time step has negligible effect on the observation. Numerical integration is always initialized with $x_1 = 20$, $x_2 = 0$ and $x_3 = -20$, and then some time (10^3 time steps) is waited before measuring observables of interest.

In all cases we have analyzed the limit cycle in the phase space $L_1(t) = x_2(t) - x_1(t)$ versus $L_2(t) = x_3(t) - x_2(t)$. Another observable containing relevant information about the trajectory of the swimmer is the center of mass evolution $x_{cm}(t) = [x_1(t) + x_2(t) + x_3(t)]/3$. The swimming velocity is measured using the best linear fit $x_{cm}(t) = vt$ over an observation of duration 10^5 s. Information about the fluctuations with respect to the average trajectory is obtained through the mean squared displacement $msd(\tau) = \langle [x_{cm}(t_0 + \tau) - x_{cm}(t_0) - v\tau]^2 \rangle$. Whenever we observe $msd(\tau) \sim 2D\tau$ for large τ, we extract D as the diffusivity of the trajectory. If the trajectory is not long enough, exceptions to the linear asymptotic behavior are observed, which are explained in the next section. We also measure the energy consumption of the swimmer in terms of the motor forces $F_i^{\text{act}}(t)$, that is, the Euler-discretized integral

$$W(t) = \int_0^t \sum_i dx_i(s) F_i^{\text{act}}(s), \tag{27}$$

which is fitted at large times as $W(t) \sim \dot{W} t$. The number $\dot{W}$ is taken as a measurement of the average energy consumption rate.

To conclude, we have measured the precision rate of each long trajectory by the formula

$$p = \frac{v^2}{D}, \tag{28}$$

which is expected to satisfy the thermodynamic uncertainty relation [20,21,44–46]

$$p \leqslant p_{\max} = \frac{\dot{W}}{k_B T}. \tag{29}$$

G. Mean squared displacement

We conclude this introductory section by briefly discussing the behavior of $msd(\tau)$ as a function of the delay τ. As shown in Fig. 5, we observe that when the temperature T is large enough, one always has a clear asymptotic diffusive behavior. On the contrary, when the temperature T is too small, the mean squared displacement oscillates with a frequency which is equal to the swimming force frequency $\omega/(2\pi)$ and an amplitude which tends to reduce with τ. The oscillations occur around a time-dependent shape which is asymptotically linear in time, therefore it is possible to extract a diffusivity D even in this case.

The reason for such an oscillating behavior is the presence of the oscillating forces which, when the noise is not large enough, dominate on the dynamics and give an observable recurrency in the trajectory.

III. NUMERICAL STUDY

In this section we present the results of the numerical simulations. Each of the following subsections is devoted to the effect of one particular physical parameter upon the most relevant observables of our study, which are the average velocity of the center of mass, the average consumption rate of energy, the diffusivity, and the precision.

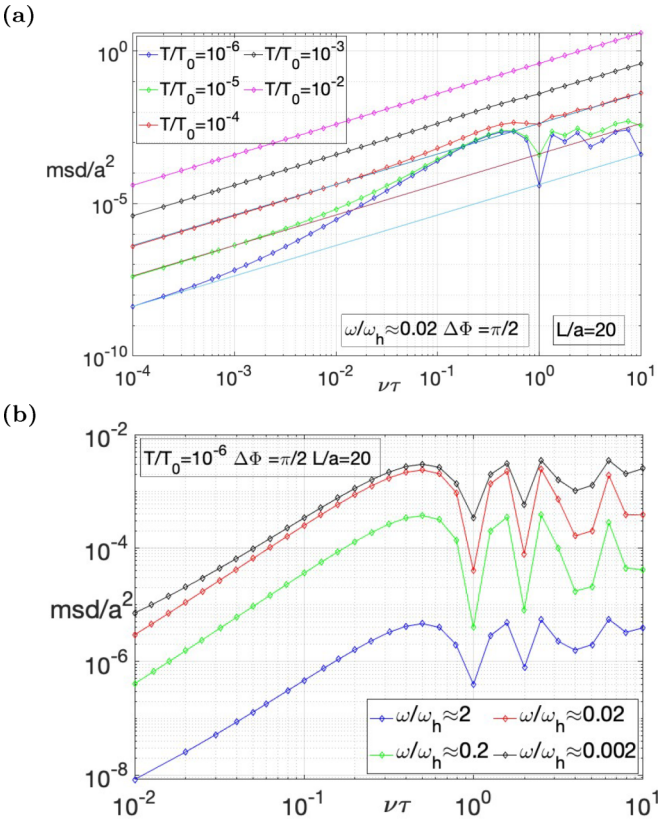

FIG. 5. Mean squared displacement as a function of time for several choices of temperatures (a) and frequencies of the active force (b). Parameters which are not given in the figure: $L = 20$, $F_0 = 10$, $a = 1$, $\eta = 1$, $K = 2$. All the straight lines in (a) have slope 1, representing the diffusive regime.

A. Changing the active force

The active force defined in Eq. (10) has three parameters: F_0, ω, and $\Delta\phi$. In Fig. 6 we study the effect of ω, while in Fig. 7 we consider $\Delta\phi$. Since the theoretical part (Sec. V)

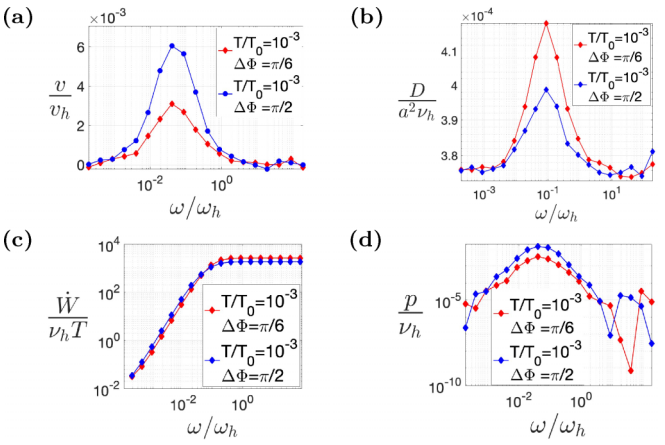

FIG. 6. Effect of the frequency of the oscillating active force ω upon (a) the average swim velocity, (b) the swimming diffusivity, (c) the energy consumption rate, and (d) the precision. Parameters: $L = 20$, $F_0 = 10$, $a = 1$, $\eta = 1$, $K = 2$.

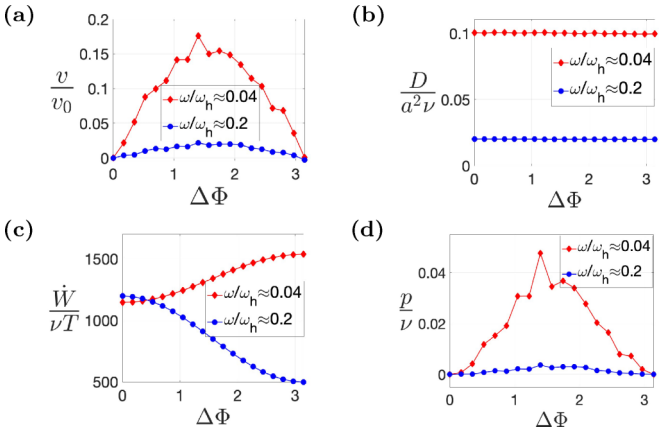

FIG. 7. Effect of the phase difference among the first and last components of the oscillating active force $\Delta\phi$ upon (a) the average swim velocity, (b) the swimming diffusivity, (c) the energy consumption rate, and (d) the precision. Parameters: $L = 20$, $F_0 = 10$, $a = 1$, $\eta = 1$, $K = 2$, $T/T_0 = 10^{-2}$.

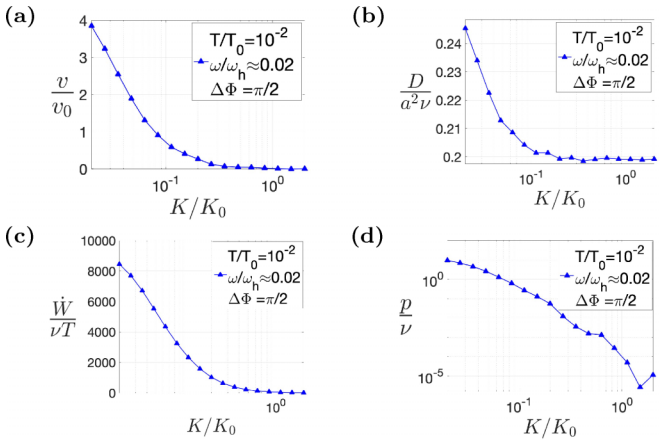

FIG. 8. Effect of the elastic constant of the confining potential K upon (a) the average swim velocity, (b) the swimming diffusivity, (c) the energy consumption rate, and (d) the precision. Parameters: $L = 20$, $F_0 = 10$, $a = 1$, $\eta = 1$.

focuses on linear response, the effect of F_0 in this regime is trivial and we do not investigate it.

Both average velocity and diffusivity have an optimum at a similar frequency $\omega_{\rm opt}$, apparently independent of $\Delta\phi$. Note that the excursion between the peak value and the base value (i.e., at small and large frequencies) is large for v but only of order 20% for the diffusivity (in fact, diffusivity has a finite value even when there is no drift or work). The work rate grows with frequency and saturates at large frequency. The behavior in frequency of work rate and average velocity is qualitatively similar to the response of a driven resonant oscillator: when the perturbation frequency is much smaller than the resonant frequency, the oscillator follows the perturbation (and then the velocity and the work rate decrease when the frequency decreases); when it is much faster, the oscillator cannot follow it, therefore the velocity reduces and the work rate becomes independent from the frequency [37]. A qualitative picture can be grasped by considering the competition of two characteristic time scales: that of the perturbation $2\pi/\omega$ and that of the (damped) harmonic binding potential $a\eta/K$. We note that this resonant behavior is substantially different from that observed in the original model (kinematically driven and without confining springs), where one simply has $v \sim \omega$, see Eq. (9). We rationalize this resonant behavior in the linear (small force) limit, discussed in the last section.

The precision has an optimum at a similar frequency $\sim\omega_{\rm opt}$, since it is dominated by the numerator v^2. The phase difference has quite a small (order of a few percent points), apparently monotonous, effect on the diffusivity, while it is relevant for the average velocity, having a peak at $\Delta\phi = \pi/2$: clearly there is no swimming when $\Delta\phi = 0$ or π, since in both cases the perturbation force vector becomes symmetric under the time-reveral operation. The effects on both v and D are weakly dependent upon ω. The work rate, on the contrary, has a dependence on $\Delta\phi$, e.g., decreasing or increasing, that changes with the value of ω. The precision, which is dominated by v^2, follows a similar graph with an optimum at $\pi/2$.

B. Changing the properties of the confining potential

The effect of the elastic constant K for the confining potential is shown in Fig. 8. All the quantities of interest decay with K. Numerically, it is not possible to decrease too much the value of K, since it leads to too large excursion of the distances between the particles and therefore to the possibility of two of them to touch each other, breaking the condition of non small distance and to a numerical instability of the mobility matrix. which contains inverse powers of the distances.

We also consider the effect of changing $L = l_1 = l_2$, the rest distance among the swimmer particles. The consequence of changing L is similar to that of changing K, see Fig. 9. The analogy between these two parameters can be understood in the following way. At fixed L the effect of reducing K is to permit larger excursions of $x_1 - x_2$ and $x_2 - x_3$ with respect to their rest value L, but such excursions include both large values (which are irrelevant) as well as small values, where

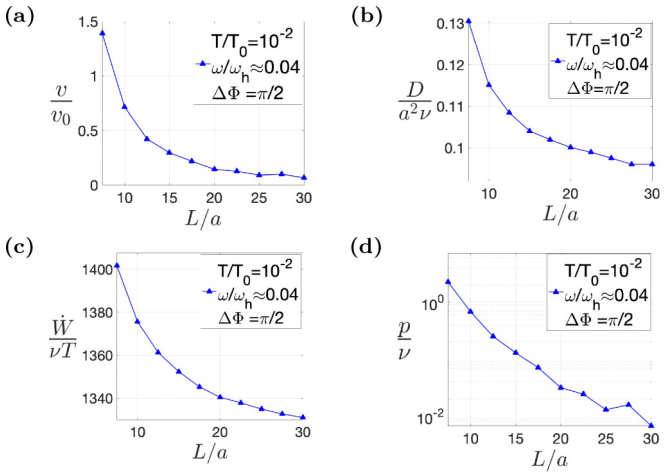

FIG. 9. Effect of the average length of the two arms of the swimmer L upon (a) the average swim velocity, (b) the swimming diffusivity, (c) the energy consumption rate, and (d) the precision. Parameters: $a = 1$, $F_0 = 10$, $\eta = 1$, $K = 2$.

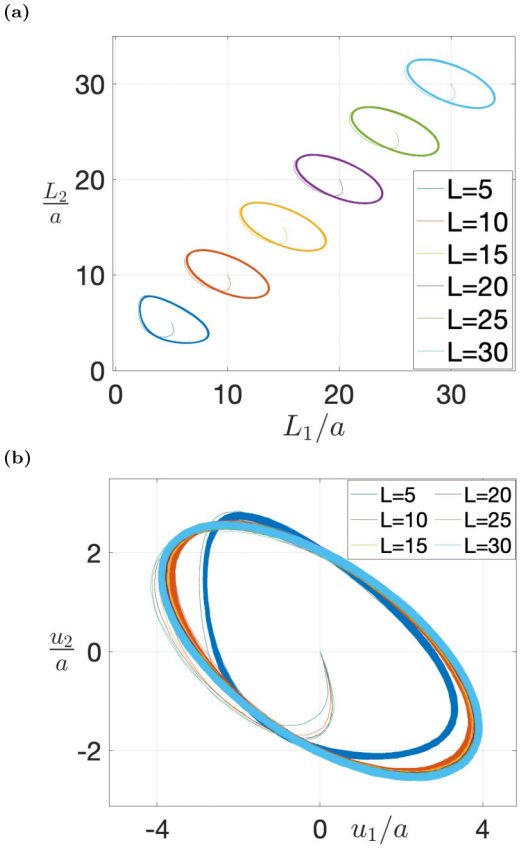

FIG. 10. Effect of the average length of the two arms of the swimmer L upon the orbits in the plane $x_1 - x_2, x_2 - x_3$ (a) and u_1, u_2 (b), where $u_1 = x_1 - x_2 - L$ and $u_2 = x_2 - x_3 - L$. Parameters: $a = 1$, $F_0 = 10$, $\eta = 1$, $T = 0.01$, $\Delta\phi = \pi/2$, $\omega = 2\pi/50$, $K = 2$.

the hydrodynamic interaction is stronger and the swimming efficiency is higher. The same occurs when L is reduced at fixed K. Of course, this analogy is qualitative, while the quantitative behavior is more complex.

In Fig. 10 we also show the orbits in the plane of relative distances (with or without shifting by the rest length L) when L is varied. This figure shows a remarkable robustness of the shape of the limit cycle which appears independent of L for large enough L. As already discussed, see Eq. (9), the average velocity of the swimmer is proportional to the area of the limit cycle with a proportionality factor $\alpha \sim L^{-1}$, therefore the behavior $v \sim L^{-1}$ is compatible with the observed orbital invariance. It is less clear how the observed orbital invariance may be related to the weak dependence of the work rate with L. As made clear in the Appendix, the explicit dependence of v and $\dot{W}$ on $L = l_1 = l_2$ is hard to read explicitly.

C. Changing the properties of the fluid

The fluid is characterized by viscosity η and temperature T. As shown in the equations of motion (18), there is not a trivial rescaling of time or positions with η or T, unless in the noiseless limit $T \to 0$, where time can be safely rescaled with η. Therefore, Figs. 11 and 12 show the genuine effect of noise on the system. Both velocity and diffusivity decrease

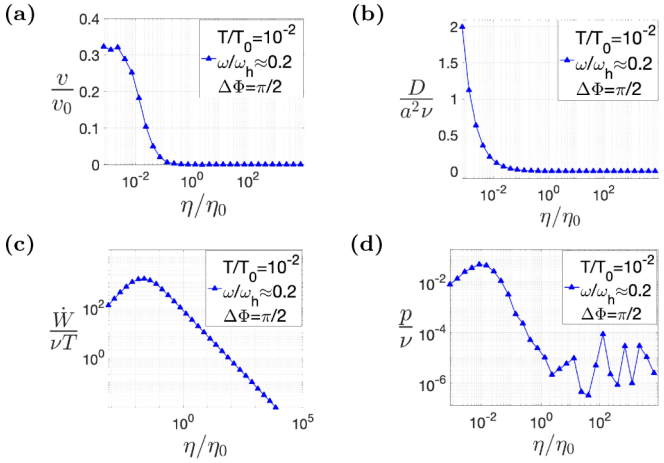

FIG. 11. Effect of the viscosity of the fluid η upon (a) the average swim velocity, (b) the swimming diffusivity, (c) the energy consumption rate, and (d) the precision. Parameters: $L = 20$, $F_0 = 10$, $a = 1$, $K = 2$.

with η, however the first seems to reach a constant value for small viscosities. Work rate and precision have a maximum for a similar viscosity value. The nonmonotonous behavior of the work rate is well reproduced by the analysis—obtained in the linear approximation—exposed in Sec. V and in the Appendix. Such a nonmonotonicity with the viscosity has been noticed before in Refs. [47,48].

Easier to read, at least on the empirical side, is the behavior of the relevant observables with T, see Fig. 12. The average velocity is apparently independent of T, and so is the work rate. Diffusivity grows linearly with T, as in the simplest scenario of an effective noise which is proportional to the amplitude of the single particle noises, and as a consequence, the precision decreases as $1/T$ for the same reason.

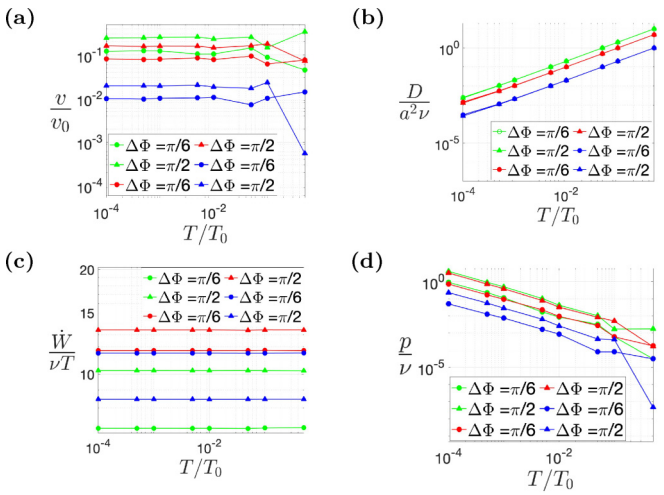

FIG. 12. Effect of the temperature of the fluid T upon (a) the average swim velocity, (b) the swimming diffusivity, (c) the energy consumption rate, and (d) the precision. Parameters: $L = 20$, $F_0 = 10$, $a = 1$, $\eta = 1$, $K = 2$. Plots in green: $\omega/\omega_h \approx 0.02$, plots in red: $\omega/\omega_h \approx 0.04$, plots in blue: $\omega/\omega_h \approx 0.2$.

IV. EFFICIENCY THROUGH THE THERMODYNAMIC UNCERTAINTY RELATION

In view of the thermodynamic uncertainty relation, Eq. (29), we are interested in the TUR-based efficiency

$$e_{\rm TUR} = \frac{p}{p_{\rm max}} = \frac{v^2 k_B T}{D\dot{W}} \leqslant 1, \tag{30}$$

which is a figure of merit with respect to the maximum achievable swimming precision.

Let us briefly discuss also energetic efficiency. For an engine, its most direct definition is the ratio between energy produced and energy spent. The problem, with a simple swimmer such as ours, is that it obeys, in the steady state, a balance between external forces and hydrodynamic resistance, therefore between spent work and produced energy (the confining potential constitutes an exact difference which vanishes along stationary averages), leading to efficiency 1. It makes sense, therefore, to consider the so-called "low-Re swimming efficiency" e_L given by

$$e_L = \frac{v\mathcal{F}}{\dot{W}}, \tag{31}$$

where $\mathcal{F}$ is the force required to drag a rigid body (with some property shared with our swimmer, e.g., shape, size, etc.) at the time-averaged swimming velocity v, while $\dot{W}$ is the average rate of work done by the active forces $\dot{W} = \langle \sum_i \dot{x}_i F_i^{\rm act} \rangle$ in the stationary swimming regime. The drag force can be put in a general form valid for low-Re regimes, i.e., $\mathcal{F} = 6\pi\eta a_{\rm eff} v$, where η is the fluid viscosity and $a_{\rm eff}$ is an effective radius which we set to L. In principle, E does not have to be less than one, but for many cases—particularly in biology—it is smaller than 1, typically of order 1%, and therefore it is generally regarded as an efficiency or as a figure of merit. It is sometimes called Lighthill efficiency or Froude efficiency [49,50].

We immediately note that there is a simple connection between hydrodynamic efficiency and TUR-based efficiency:

$$e_L = e_{\rm TUR} \frac{6\pi\eta a_{\rm eff} D}{k_B T}, \tag{32}$$

so that when $D = k_B T/(6\pi\eta a_{\rm eff})$, one has $e_{\rm TUR} = e_L$.

In Fig. 13 we display the TUR-based efficiency $e_{\rm TUR}$ with its dependence upon the six parameters of the model we have considered so far. Our first remark is that the precision of the model is, in general, smaller than the allowed maximum by several orders of magnitude. The highest observed values of $e_{\rm TUR}$ are obtained for small K and small L and are of the order of 10^{-3}.

The efficiency is weakly dependent upon $\Delta\phi$, with an optimum around $\pi/2$. It does not depend evidently on ω when $\omega < \omega_{\rm opt}$ (we recall that $\omega_{\rm opt}$ is where the velocity and the precision are highest); however, the efficiency rapidly decreases with ω when it is larger than $\omega_{\rm opt}$. It is difficult to validate the apparent growth of $e_{\rm TUR}$ for very high frequencies, but it could be just wide fluctuations induced by the strong noise affecting diffusivity and, as a consequence, precision; see Fig. 6.

The efficiency decreases when both K and L are increased, but the effect of K is soft (i.e., $e_{\rm TUR} \sim 1/K$) while the effect of L is relevant, e.g., it decreases by two orders of magnitude,

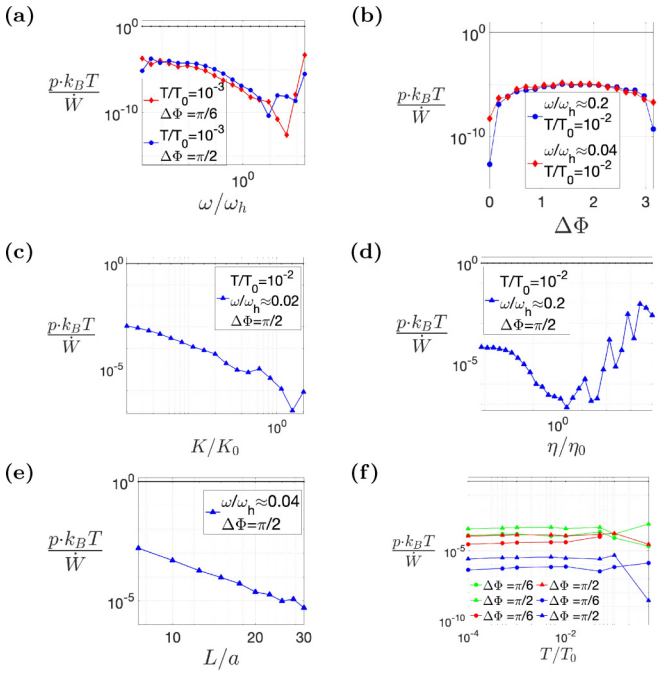

FIG. 13. Effect of the physical parameters upon the TUR-based $e_{\rm TUR}$ efficiency. Parameters where not specified: $L = 20$, $F_0 = 10$, $a = 1$, $\eta = 1$, $T = 0.01$, $\Delta\phi = \pi/2$, $\omega = 2\pi/50$, $K = 2$. Plots in black: $pk_B T/\dot{W} = 1$.

increasing L by less than a factor 4. Such an observation seems to contradict a recent study on the Lighthill efficiency of the original three-beads model [51]; however, a direct comparison is not correct: in the original model, in fact, the L parameter represents the maximum extension of the swimmer's arms, which is externally imposed, while in our case L is the length at rest of the arms, while the real excursion of their length is dictated by the dynamics under the effect of the active forces and the harmonic confinement.

The efficiency has an almost negligible dependence upon the fluid temperature, however it becomes very noisy for large values of T. The effect of the fluid viscosity η is surprisingly nonmonotonic, with a minimum at values of viscosity between 10 and 10^2, which (under the conversion discussed in Sec. II D) corresponds roughly to water viscosity.

V. ANALYTICAL STUDY FOR SMALL DEFORMATION

In this last section we discuss an analytic approach mainly focused to the computation of the average velocity of the swimmer model considered here, which—even without noise—is different from the original model for the presence of the confining potential. In the final part of this section we also discuss zero-order approximations for their diffusivity and, consequently, their thermodynamic precision. A full treatment of the stochastic problem is left to a future study.

A. Linearized equations for the average motion

We define $L_1(t) = l_1 + u_1(t)$ and $L_2(t) = l_2 + u_2(t)$. The equation of motion, Eq. (18) after averaging over noise, reads,

for small u_1, u_2

$$\underline{v} = \mathbf{T} \cdot \underline{F} \approx (\mathbf{T}_0 + \mathbf{T}_1)(\underline{F}^{\rm act} + \underline{F}^{\rm pot}) + (\underline{F}_{\rm Ito,0} + \underline{F}_{\rm Ito,1}). \tag{33}$$

In fact, in the small u_1, u_2 limit we can expand the mobility matrix:

$$\mathbf{T} \approx \mathbf{T}_0 + \mathbf{T}_1 \tag{34}$$

$$\mathbf{T}_0 = \begin{pmatrix} \frac{1}{6\pi\eta a} & \frac{1}{4\pi\eta l_1} & \frac{1}{4\pi\eta(l_1+l_2)} \\ \frac{1}{4\pi\eta l_1} & \frac{1}{6\pi\eta a} & \frac{1}{4\pi\eta l_2} \\ \frac{1}{4\pi\eta(l_1+l_2)} & \frac{1}{4\pi\eta l_2} & \frac{1}{6\pi\eta a} \end{pmatrix} \tag{35}$$

$$\mathbf{T}_1 = -\begin{pmatrix} 0 & \frac{u_1}{4\pi\eta l_1^2} & \frac{u_1+u_2}{4\pi\eta(l_1+l_2)^2} \\ \frac{u_1}{4\pi\eta l_1^2} & 0 & \frac{u_2}{4\pi\eta l_2^2} \\ \frac{u_2}{4\pi\eta(l_1+l_2)^2} & \frac{u_2}{4\pi\eta l_2^2} & 0 \end{pmatrix}. \tag{36}$$

Also, the Ito forces can be expanded at first order in u_1, u_2:

$$\underline{F}_{\rm Ito} \approx \underline{F}_{\rm Ito,0} + \underline{F}_{\rm Ito,1} \tag{37}$$

$$\underline{F}_{\rm Ito,0} = \frac{1}{\beta}\frac{1}{4\pi\eta}\begin{pmatrix} \frac{1}{(l_1+l_2)^2} + \frac{1}{l_1^2} \\ \frac{1}{l_2^2} - \frac{1}{l_1^2} \\ \frac{1}{(l_1+l_2)^2} + \frac{1}{l_2^2} \end{pmatrix} \tag{38}$$

$$\underline{F}_{\rm Ito,1} = \frac{1}{\beta}\frac{1}{4\pi\eta}\begin{pmatrix} -2\left(\frac{u_1}{l_1^3} + \frac{u_1+u_2}{(l_1+l_2)^3}\right) \\ 2\left(\frac{u_1}{l_1 l_2^2} - \frac{u_2}{l_2^3} + \frac{u_1}{l_1^3} - \frac{u_2}{l_2 l_1^2}\right) \\ 2\left(\frac{u_2}{l_2^3} + \frac{u_1+u_2}{(l_1+l_2)^3}\right) \end{pmatrix}. \tag{39}$$

We note that the Ito forces $\underline{F}_{\rm Ito,i}$ contains terms of order $1/l^2$ and u/l^3, where l is l_1 or l_2. All these terms are smaller than the terms $1/l$ and u/l^2 contained in the expansion of $\mathbf{T}$, therefore at our level of approximation we can drop the Ito forces. Also, the term $\mathbf{T}_1 \cdot \underline{F}^{\rm pot}$ can be dropped as it is of order $\sim u^2$.

Finally, the above equation can be put in the form of an equation for the time derivative of the only two relevant degrees of freedom u_1, u_2, i.e.,

$$\dot{u}_1 = v_1 - v_2, \quad \dot{u}_2 = v_2 - v_3, \tag{40}$$

with time-dependent forces reduced to only two components $\underline{f}^{(2)}_{\rm act}(t) = [F_1^{\rm act}(t), F_3^{\rm act}](t)$, obtaining

$$\dot{\underline{u}}(t) = [\mathbf{M}_1(t) + \mathbf{M}_2]\underline{u}(t) + \mathbf{M}_3 \cdot \underline{f}^{(2)}_{\rm act}, \tag{41}$$

with

$$\mathbf{M}_1(t) = -\frac{1}{4\eta\pi}\begin{pmatrix} \frac{-f_3^{\rm act}(t)}{l_{12}^2} - \frac{2f_1^{\rm act}(t)}{l_1^2} & -\frac{f_3^{\rm act}(t)}{l_{21}^2} \\ \frac{f_1^{\rm act}(t)}{l_{12}^2} & \frac{2f_3^{\rm act}(t)}{l_2^2} + \frac{f_1^{\rm act}(t)}{l_{21}^2} \end{pmatrix}, \tag{42}$$

where $1/l_{12}^2 = 1/l_1^2 - 1/(l_1+l_2)^2$ and $1/l_{21}^2 = 1/l_2^2 + 1/(l_1+l_2)^2$.

$$\mathbf{M}_2 = -\frac{K}{\eta\pi}\begin{pmatrix} \frac{1}{3a_1} & -\frac{1}{6a_{12}} \\ -\frac{1}{6a_{12}} & \frac{1}{3a_2} \end{pmatrix}, \tag{43}$$

where $1/(3a_1) = 1/(3a) - 1/(2l_1)$, $1/(3a_2) = 1/(3a) - 1/(2l_2)$, $1/6a_{12} = 1/(6a) - 1/(4l_1) - 1/(4l_2) + 1/[4(l_1 + l_2)]$, and finally,

$$\mathbf{M}_3 = \frac{1}{\eta\pi}\begin{pmatrix} \frac{1}{3a_1} & \frac{1}{6a_{12}} \\ -\frac{1}{6a_{12}} & -\frac{1}{3a_2} \end{pmatrix}. \tag{44}$$

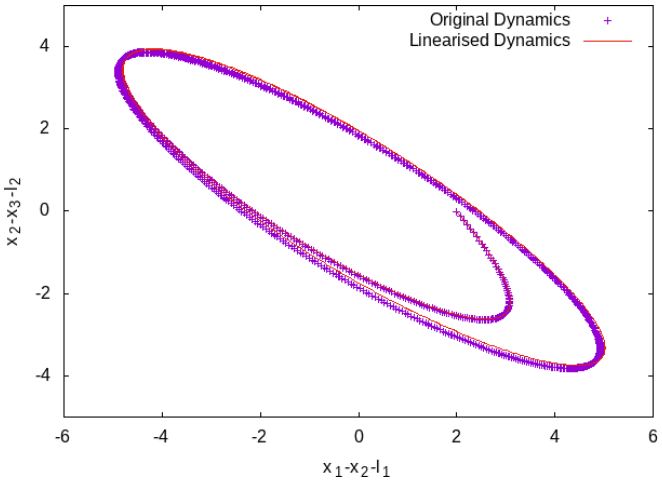

FIG. 14. Comparison of the numerical solution of Eq. (41) with that of the original model. The figure shows the limit cycle in which the displacements u_1, u_2 stay. Parameters are $L = 20$, $F_0 = 10$, $a = 1$, $\eta = 1$, $\Delta\phi = \pi/4$, $\omega = 2\pi/50$, $K = 2$.

Before proceeding with the analytical calculations, we have verified the fairness of the linear assumption, by comparing the numerical solution of Eq. (41) with that of the original model; see, for instance, Fig. 14. The overlap is almost perfect.

B. Instability without the confining potential

Let us consider the case where $K = 0$, i.e., there is no confining potential.

In this case one has that, assuming a limit cycle $\underline{u}_0(t)$ which satisfies $\dot{\underline{u}}_0 = \mathbf{M}_1\underline{u}_0 + \mathbf{M}_3\underline{f}^{(2)}_{\rm act}(t)$, then small deviations from it $\delta\underline{u}(t) = \underline{u}(t) - \underline{u}_0(t)$ obey the homogeneous equation $\dot{\delta\underline{u}} = \mathbf{M}_1\delta\underline{u}$, and therefore the stability of the cycle is dictated by the eigenvalues of $\mathbf{M}_1(t)$, which are, however, time dependent, i.e., they depend upon the values of $f_1^{\rm act}(t)$ and $f_3^{\rm act}(t)$. In principle, the limit cycle stability should be determined by studying the eigenvalues of the associated Poincaré map of the cycle which depend upon the eigenvalues along the full period of the force oscillation. This problem is simplified here since, along the whole force cycle, one of the two eigenvalues is always positive, while the other is always negative. The full analytic formula for the eigenvalues is pretty long and can be found in the Appendix. It is simplified in the case $l_1 = l_2 = L$ and takes the form

$$\lambda_{+-} = \frac{3F_1^{\rm act} - 5F_3^{\rm act} \pm \sqrt{169F_1^{\rm act} + 226F_3^{\rm act}F_1^{\rm act} + 121F_3^{\rm act}}}{32\pi\eta L^2} \tag{45}$$

The plot of eigenvalues for a particular choice of the parameter, as a function of $F_1^{\rm act}, F_3^{\rm act}$ can be found in Fig. 15.

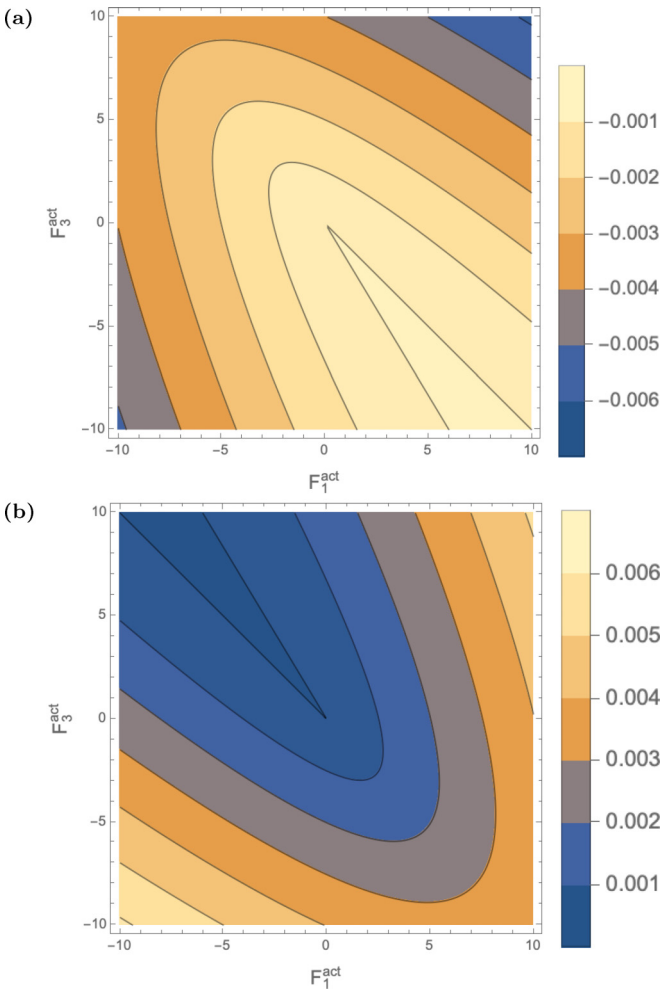

FIG. 15. Eigenvalues (a: smaller, b: larger) of the linearized dynamics, as functions of F_1^{act}, F_3^{act} when there is no elastic potential, i.e., when $K = 0$. Parameters are $L = 20$, $a = 1$, $\eta = 1$.

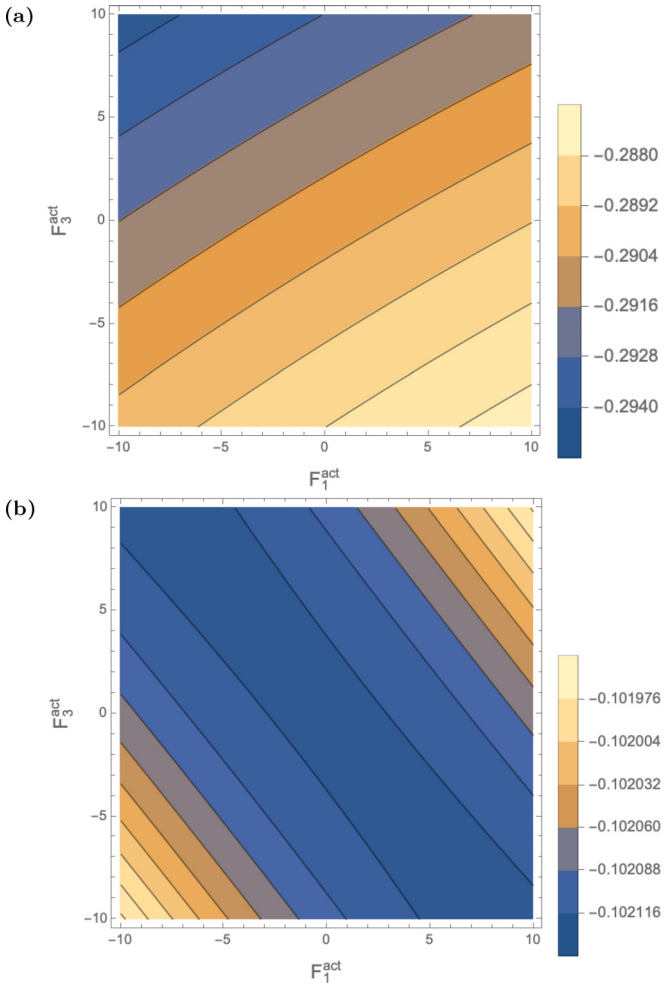

FIG. 16. Eigenvalues of the linearized dynamics (a: smaller, b: larger), as functions of F_1^{act}, F_3^{act} in the presence of elastic potential. Parameters are $L = 20$, $a = 1$, $\eta = 1$, $K = 2$.

When also M_2 is considered, i.e., $K > 0$, then the stability is restored as both eigenvalues become negative, as shown in Fig. 16.

C. Solution for the limit cycle

A further simplification can be operated on Eq. (41), by considering that when $F^{act} = 0$ (and $K > 0$), the limit cycle becomes a stable fixed point with $u_1 = u_2 = 0$. This implies that one may expect u_1, u_2 to be—for small F^{act}—of the same order of F^{act}, and therefore the term $\mathbf{M}_1(t)\underline{u}$ is of order $(F^{act})^2 \approx \underline{u}^2$ and can be dropped in our small deviations treatment. It is therefore easy to get a solution for the remaining system of equation; the strategy and the detailed results are given in the Appendix. Here we report the expression for the average velocity of the swimmer in the symmetric case $l_1 = l_2 = L = \ell a$:

$$v = \frac{\alpha}{2} F_0^2 \, Q(K, a\eta\omega, \ell)\, \omega \, \sin(\Delta\phi), \tag{46}$$

where we recall, for simplicity, the expression for α in the symmetric case:

$$\alpha = \frac{7}{12}\frac{a}{L^2}, \tag{47}$$

and the function $Q(K, a\eta\omega, \ell)$, which takes the form

$$Q = -\frac{q_1 q_2 [q_3 a^2\eta^2\omega^2 + q_1 q_2 K^2]}{[q_4 a^2\eta^2\omega^2 + q_1^2 K^2][q_5 a^2\eta^2\omega^2 + q_2^2 K^2]}, \tag{48}$$

with $q_1 = 4\ell - 7$, $q_2 = 4\ell - 3$, $q_3 = 192\pi^2\ell^2$, $q_4 = 64\pi^2\ell^2$, and $q_5 = 576\pi^2\ell^2$. Consistently with the anticipated qualitative picture, the factor Q depends upon the main parameters of the model K, ω, a, and η uniquely through the combination $\omega a\eta/K$, which is the ratio between the two characteristic time scales: that of the perturbation $1/\omega$ and that of the (damped) harmonic binding potential $a\eta/K$.

Comparing Eqs. (46) with (9), we note that the product $d_1 d_2$ is replaced by $F_0^2 Q$, which measures the quadratic amplitude of the oscillations of the distances between the spheres. This amplitude is maximum when the frequency of the internal forces is comparable to the characteristic relaxation

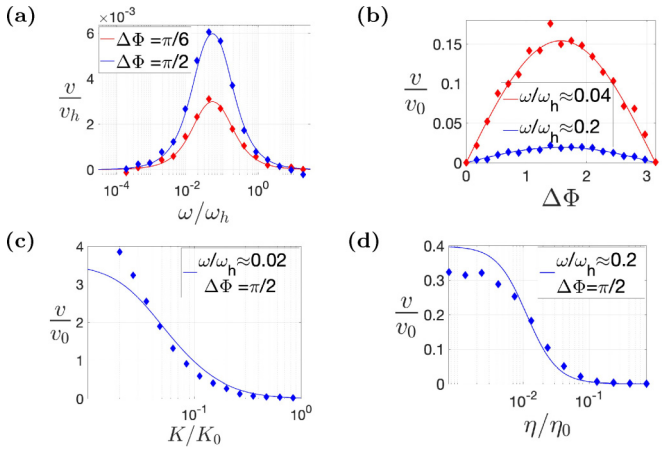

FIG. 17. Theoretical behavior of average velocity with respect to (a) frequency ω, (b) phase difference $\Delta\phi$, (c) stiffness coefficient K, and (d) viscosity η. Where not specified, the parameters are $L = 20$, $a = 1$, $\eta = 1$, $K = 2$.

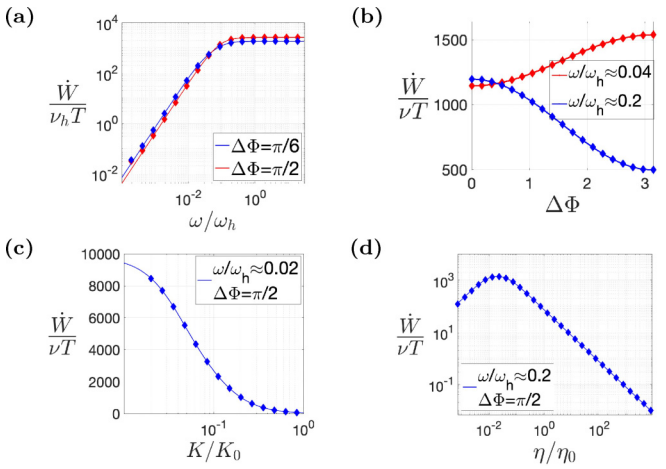

FIG. 18. Theoretical behavior of average work rate with respect to (a) frequency ω, (b) phase difference $\Delta\phi$, (c) stiffness coefficient K, and (d) viscosity η. Where not specified, the parameters are $L = 20$, $a = 1$, $\eta = 1$, $K = 2$.

rates of the system, which appear in the denominator of the formula (46).

The plots of the analytical estimate of v versus the main parameters of the model are shown in Fig. 17, and a comparison with the numerical results in the previous sections is excellent.

We can also obtain an expression for the average work rate which, putting the internal force condition and the definition of u_1, u_2 in the definition of W, Eq. (27), reads

$$\dot{W} = \frac{1}{\mathcal{T}} \int_0^{\mathcal{T}} dt[-F_1(t)\dot{u}_1(t) + F_3(t)\dot{u}_2(t)]. \tag{49}$$

Explicit formulas for all the parameters are shown in the Appendix, but in the symmetric case $l_1 = l_2 = \ell a$ we get

$$\dot{W} = \frac{8\pi a\eta F_0^2 l\omega^2[\cos(\Delta\phi)W_1 + W_2]}{W_3}, \tag{50}$$

with $W_1 = w_1 a^2\eta^2\omega^2 - w_2 K^2$, $W_2 = w_3 a^2\eta^2\omega^2 + w_4 K^2$, $W_3 = w_5 a^4\eta^4\omega^4 + w_6 a^2\eta^2 K^2\omega^2 + w_7 K^4$ and with $w_1 = 192\,\pi^2\ell^2(4\ell - 9)$, $w_2 = (4\ell - 7)(4\ell - 3)(4\ell - 9)$, $w_3 = 768\,(2l - 3)\pi^2\ell^2$, $w_4 = 4(2l - 3)(4\ell - 7)(4\ell - 3)$, $w_5 = 36\,864\,\pi^4\ell^4$, $w_6 = 128\pi^2\ell^2[8l(10l - 33) + 225]$, $w_7 = (3 - 4l)^2\,(7 - 4l)^2$. The plots of the analytical estimate of $\dot{W}$ versus the main parameters of the model are shown in Fig. 18. Again, the qualitative comparison with the numerical results in the previous sections is excellent, and the quantitative one is also quite fair.

D. Estimates for the diffusivity, precision, and efficiency

While the swimming velocity in the limit cycle can be estimated by using the average equation, i.e., neglecting noise terms, the diffusivity cannot: in our case, where the noise is multiplicative, a consistent estimate becomes a hard job. Numerical evidence suggests that the diffusivity is only weakly dependent upon the parameters of the swimmer: with ω and ϕ it varies less than 10%, while with L and K it varies less than 50%. The fluid properties obviously have a much stronger influence on D, but such influence is trivial; in fact, it is seen that $D \sim T/\eta$, as it is implied by the coefficient $\approx \sqrt{T_{ij}/\beta} \sim \sqrt{\frac{T}{\eta}}$ in front of the noise, see Eq. (18). In this section we discuss a "zero order" approximation for D.

The diffusivity of the center of mass D is deduced from the knowledge of the asymptotic behavior of the mean squared displacement:

$$msd(t) = \langle [x_{c_m}(t) - x_{c_m}(0) - \bar{\dot{x}}_{c_m} t]^2 \rangle = \left\langle \left[\int_0^t ds\, \Delta\dot{x}_{c_m}(s) \right]^2 \right\rangle \xrightarrow[t\to\infty]{} 2Dt. \tag{51}$$

We follow the idea of the previous sections and get a formal expansion (in powers of displacements u_i) for the equations of motion including noise,

$$\dot{x}_i = \mathbf{T}_{ij} f_j^{\text{tot}} = \underbrace{\mathbf{T}^0_{ij} f^{el}_j + \mathbf{T}^0_{ij} f^{\text{act}}_j + \mathbf{T}^1_{ij} f^{\text{act}}_j}_{\text{deterministic average velocity}} + \underbrace{\left(\mathbf{T}^0_{ij} + \mathbf{T}^1_{ij}\right) \underbrace{\sqrt{\frac{2}{\beta}} \left(\Sigma^0_{jk} + \Sigma^1_{jk}\right) \eta_k}_{f^n_j}}_{\Delta\dot{x}_{c_m}}, \tag{52}$$

where

$$\sqrt{\zeta} = \Sigma \sim \Sigma^0 + \Sigma^1 + \cdots, \tag{53}$$

and leading to

$$msd(t) = \left\langle \left[\int_0^t ds \sum_{ijk} \frac{\mathbf{T}^0_{ij} + \mathbf{T}^1_{ij}}{3} \sqrt{\frac{2}{\beta}} \left(\Sigma^0_{jk} + \Sigma^1_{jk}\right) \eta_k \right]^2 \right\rangle.$$

The first-order terms are time dependent and make the calculations more involved as they imply to integrate the solutions for $u(t)$, including their fluctuations. For this reason, we keep

only the zeroth-order term:

$$\left\langle \left[\int_0^t ds \frac{\sum_{ijk} \mathbf{T}^0_{ij}}{3} \sqrt{\frac{2}{\beta}} \Sigma^0_{jk} \eta_k \right]^2 \right\rangle = \frac{1}{9} \left\langle \int_0^t ds \int_0^t ds' \left[\sum_k \sqrt{2D_k} \eta_k(s) \sum_l \sqrt{2D_l} \eta_l(s') \right] \right\rangle, \tag{54}$$

with

$$\langle \eta_k(s) \eta_l(s') \rangle = \delta_{kl} \delta(s - s'), \tag{55}$$

and

$$\sqrt{D_k} = \frac{1}{\sqrt{\beta}} \sum_i [\mathbf{T}^0 \Sigma^0]_{ik}. \tag{56}$$

In conclusion, we get

$$msd(t) = \frac{1}{9} \sum_k \int_0^t ds \int_0^t ds' 2D_k \, \delta(s - s') = 2Dt, \tag{57}$$

with

$$D = \frac{1}{9} \sum_k D_k. \tag{58}$$

In the case $l_1 = l_2 = L$ and in the limit $a \ll L$, one has $\Sigma^0 = \sqrt{6\pi \eta a}\, \mathcal{I}$ and therefore $D_k = 1/(6\pi \eta a \beta)\, \mathcal{I}$, leading to

$$D = \frac{D_0}{3} \tag{59}$$

with

$$D_0 = \frac{1}{6\pi \eta a \beta}, \tag{60}$$

the bare diffusivity of a single sphere. With $\eta = 1$ and $a = 1$, this crude estimate gives $D \approx 0.018T$, which agrees with the leading value observed in the numerical simulations with those parameters, see Figs. 6–9.

Remarkably, simple calculations show that

$$D \approx D_0 \left\{ \frac{1}{3} + \frac{5}{6} \frac{a}{L} + O\left[\left(\frac{a}{L} \right)^2 \right] \right\}. \tag{61}$$

Therefore, at small but finite a and L, the hydrodynamic couplings *increase* the diffusivity.

VI. CONCLUSIONS AND PERSPECTIVES

We have studied numerically and analytically the three-beads swimmer model with two important modifications: thermal noise and a confining potential. The latter is physically but also mathematically motivated, since the original model, if solved dynamically (i.e., imposing the driving forces and observing the resulting trajectory), is unstable: the three particles do not remain in a close neighborhood, which is necessary for hydrodynamic interactions to couple their dynamics and prevent reciprocal motion i.e., time reversibility and vanishing of the swimming effect. The introduction of noise makes it possible to measure the swimming precision, constrained by the thermodynamic uncertainty relation. It has, however, no evident effects on the average dynamics of the swimmer, as it can be deduced by the graphs of the observables in temperature, i.e., Figs. 12 and 13(d). The study also reveals that this model is usually far from the TUR optimal bound, but its precision efficiency can be improved by reducing the confining potential stiffness K or the length at rest of the two swimmer arms L. Future investigations should include a more general class of driving protocols, higher-order terms in the perturbative expansion for the diffusivity, and, in particular, the introduction of noise in the active force, which is perhaps a much stronger—and yet realistic—source of fluctuations for microswimmers [8]. The model can be adapted to more realistic setups and dimensions of space: the active force, for instance, can be modeled to act on a direction which is related to the actual orientation of the swimmer (if in more than one dimension) or to the surrounding swimmers in a multiparticle numerical experiment [52–54]: the effect of all these ingredients on the TUR-based efficiency e_{TUR} looks to be an interesting open problem. For the same purpose of investigating the role of precision and TUR in different regimes, the three-beads swimmer can also model microalgae such as the *C. reinhardtii* [55,56].

ACKNOWLEDGMENTS

This project has received funding from the European Research Council (ERC) under the European Union's Horizon 2020 research and innovation programme (Grant Agreement No. 834615).

APPENDIX A: LINEAR APPROXIMATION

Equation (41), keeping only the linear order in F_0, casts into

$$\dot{\underline{u}}(t) = \mathbf{M}_2 \cdot \underline{u}(t) + \mathbf{M}_3 \cdot \underline{f}^{(2)}_{\mathrm{act}}, \tag{A1}$$

which can be solved by setting

$$u_i = A_i \cos(\omega t) + B_i \sin(\omega t) \quad (i = 1, 2). \tag{A2}$$

Lengthy computations lead to the following expressions for the four coefficients:

$$A_i = \frac{\sum_{j=0}^3 A_i^j K^j (\eta\omega)^{3-j}}{\sum_{j=0}^2 A_{d,i}^j K^{2j} (\eta\omega)^{4-2j}}, \tag{A3}$$

$$B_i = \frac{\sum_{j=0}^3 B_i^j K^j (\eta\omega)^{3-j}}{\sum_{j=0}^2 B_{d,i}^j K^{2j} (\eta\omega)^{4-2j}}, \tag{A4}$$

with

$$A_1^0 = 432\pi^3 a_1 a_{12}^4 a_2^2 \sin(\Delta\phi) \quad A_1^1 = -36\pi^2 a_{12}^2 a_2 \left\{ a_1^2 [\cos(\Delta\phi) a_2 + 2a_{12}] + 4\cos(\Delta\phi) a_{12}^2 a_2 + 2a_1 a_{12} a_2 \right\}$$

$$A_1^2 = -12\pi a_1 a_{12}^2 \sin(\Delta\phi) \left(a_1 a_2 - 4a_{12}^2 \right) \quad A_1^3 = -\cos(\Delta\phi) \left(a_1 a_2 - 4a_{12}^2 \right)^2$$

$$A_{d,1}^0 = 1296\pi^4 a_1^2 a_{12}^4 a_2^2 \quad A_{d,1}^1 = 72\pi^2 a_{12}^2 \left[a_1^2 \left(2a_{12}^2 + a_2^2 \right) + 2a_{12}^2 a_2^2 \right] \quad A_{d,1}^2 = (-4a12^2 + a1a2)^2$$

$$B_1^0 = 216\pi^3 a_1 a_{12}^3 a_2^2[2\cos(\Delta\phi)a_{12} + a_1] \quad B_1^1 = 36\pi^2 a_{12}^2 a_2^2 \sin(\Delta\phi)\big(a_1^2 + 4a_{12}^2\big)$$
$$B_1^2 = -6\pi a_1 a_{12}[2\cos(\Delta\phi)a_{12} - a_2]\big(a_1 a_2 - 4a_{12}^2\big) \quad B_1^3 = \sin(\Delta\phi)\big(a_1 a_2 - 4a_{12}^2\big)^2$$
$$B_{d,1}^0 = 1296\pi^4 a_1^2 a_{12}^4 a_2^2 \quad B_{d,1}^1 = 72\pi^2 a_{12}^2\big[a_1^2\big(2a_{12}^2 + a_2^2\big) + 2a_{12}^2 a_2^2\big] \quad B_{d,1}^2 = \big(a_1 a_2 - 4a_{12}^2\big)^2$$
$$A_2^0 = -216\pi^3 a_1^2 a_{12}^3 a_2^2 b \quad A_2^1 = 36\pi^2 a_1 a_{12}^2\big\{a_2^2[2\cos(\Delta\phi)a_{12} + a_1] + 2\cos(\Delta\phi)a_1 a_{12} a_2 + 4a_1 a_{12}^2\big\}$$
$$A_2^2 = -6\pi a_1 a_{12} a_2 \sin(\Delta\phi)\big(a_1 a_2 - 4a_{12}^2\big) \quad A_2^3 = \big(a_1 a_2 - 4a_{12}^2\big)^2$$
$$A_{d,2}^0 = 1296\pi^4 a_1^2 a_{12}^4 a_2^2 \quad A_{d,2}^1 = 72\pi^2 a_{12}^2\big[a_1^2\big(2a_{12}^2 + a_2^2\big) + 2a_{12}^2 a_2^2\big] \quad A_{d,2}^2 = \big(a_1 a_2 - 4a_{12}^2\big)^2$$
$$B_2^0 = -216\pi^3 a_1^2 a_{12}^3 a_2[\cos(\Delta\phi)a_2 + 2a_{12}] \quad B_2^1 = -72\pi^2 a_1 a_{12}^3 a_2 \sin(\Delta\phi)(a_1 + a_2)$$
$$B_2^2 = -6\pi a_{12} a_2[\cos(\Delta\phi)a_1 - 2a_{12}]\big(a_1 a_2 - 4a_{12}^2\big) \quad B_2^3 = 0$$
$$B_{d,2}^0 = 1296\pi^4 a_1^2 a_{12}^4 a_2^2 \quad B_{d,2}^1 = 72\pi^2 a_{12}^2\big[a_1^2\big(2a_{12}^2 + a_2^2\big) + 2a_{12}^2 a_2^2\big] \quad B_{d,2}^2 = \big(a_1 a_2 - 4a_{12}^2\big)^2.$$

We conclude showing analytical expression for the average velocity

$$v = \frac{\alpha}{2}\,\overline{(u_1\dot{u}_2 - u_2\dot{u}_1)}, \tag{A5}$$

where

$$\begin{aligned}\overline{(u_1\dot{u}_2 - u_2\dot{u}_1)} &= \frac{1}{\mathcal{T}}\int_{t_0}^{t_0+\mathcal{T}} (u_1\dot{u}_2 - u_2\dot{u}_1)\,dt \\ &= \frac{1}{\mathcal{T}}\int_{t_0}^{t_0+\mathcal{T}} \left(u_1\dot{u}_2 - \underbrace{(u_2\dot{u}_1 + u_1\dot{u}_2)}_{\text{total derivative}} + u_1\dot{u}_2\right) dt \\ &= \frac{1}{\mathcal{T}}\int_{t_0}^{t_0+\mathcal{T}} 2\,u_1\dot{u}_2\,dt. \end{aligned} \tag{A6}$$

Through the above expressions one gets

$$v = \frac{\alpha}{2}\,\frac{F_0^2\omega\big(a_1 a_2 - 4a_{12}^2\big)\big\{\sin(\Delta\phi)\big[4a_{12}^2(9\pi^2 a_1 a_2\eta^2\omega^2 + K^2) - a_1 a_2 K^2\big] + 12\pi a_{12}^2\eta K\omega(a_1 - a_2)\cos(\Delta\phi)\big\}}{1296\pi^4 a_1^2 a_{12}^4 a_2^2\eta^4\omega^4 + 72\pi^2 a_{12}^2\eta^2 K^2\omega^2\big[a_1^2\big(2a_{12}^2 + a_2^2\big) + 2a_{12}^2 a_2^2\big] + K^4\big(a_1 a_2 - 4a_{12}^2\big)^2}, \tag{A7}$$

which, in terms of the original lengths at rest l_1 and l_2, takes the form

$$v = \frac{\alpha}{2}\,\frac{v_n}{v_d} \tag{A8}$$

with

$$\begin{aligned} v_n = {} & F_0^2\omega\big[3a^2\big(l_1^4 - 2l_1^3 l_2 - 5l_1^2 l_2^2 - 2l_1 l_2^3 + l_2^4\big) + 4al_1 l_2(l_1 + l_2)\big(l_1^2 + 3l_1 l_2 + l_2^2\big) - 4l_1^2 l_2^2(l_1 + l_2)^2\big] \\ & \times \sin(\Delta\phi)\big[48\pi^2 a^2\eta^2 l_1^2 l_2^2\omega^2(l_1 + l_2)^2 + K^2\big[-3a^2\big(l_1^4 - 2l_1^3 l_2 - 5l_1^2 l_2^2 - 2l_1 l_2^3 + l_2^4\big) - 4al_1 l_2(l_1 + l_2)\big(l_1^2 + 3l_1 l_2 + l_2^2\big) \\ & + \; 4l_1^2 l_2^2(l_1 + l_2)^2\big]\big\} + 24\pi a^2\eta K l_1 l_2\omega(l_2 - l_1)(l_1 + l_2)^2\cos(\Delta\phi)\big\} \end{aligned} \tag{A9}$$

and

$$\begin{aligned} v_d = {} & 9a^4\big[256\pi^4\eta^4 l_1^4 l_2^4\omega^4(l_1 + l_2)^4 + 32\pi^2\eta^2 K^2 l_1^2 l_2^2\omega^2(l_1 + l_2)^2\big(3l_1^4 + 6l_1^3 l_2 + 7l_1^2 l_2^2 + 6l_1 l_2^3 + 3l_2^4\big) \\ & + K^4\big(l_1^4 - 2l_1^3 l_2 - 5l_1^2 l_2^2 - 2l_1 l_2^3 + l_2^4\big)^2\big] + 24a^3 K^2 l_1 l_2\big[K^2(l_1 + l_2)\big(l_1^2 + 3l_1 l_2 + l_2^2\big)\big(l_1^4 - 2l_1^3 l_2 - 5l_1^2 l_2^2 - 2l_1 l_2^3 + l_2^4\big) \\ & - 16\pi^2\eta^2 l_1^2 l_2^2\omega^2(l_1 + l_2)^3\big(3l_1^2 + 5l_1 l_2 + 3l_2^2\big)\big] + 8a^2 K^2 l_1^2 l_2^2(l_1 + l_2)^2\big[80\pi^2\eta^2 l_1^2 l_2^2\omega^2(l_1 + l_2)^2 \\ & - K^2\big(l_1^4 - 18l_1^3 l_2 - 37l_1^2 l_2^2 - 18l_1 l_2^3 + l_2^4\big)\big] - 32aK^4 l_1^3 l_2^3(l_1 + l_2)^3\big(l_1^2 + 3l_1 l_2 + l_2^2\big) + 16K^4 l_1^4 l_2^4(l_1 + l_2)^4. \end{aligned} \tag{A10}$$

For instance, if $l_1 = l_2 = L = \ell a$, one has

$$v = -\frac{\alpha}{2}\,\frac{F_0^2(4\ell - 7)(4\ell - 3)\omega\sin(\Delta\phi)[192\pi^2 a^2\eta^2\ell^2\omega^2 + K^2(4\ell - 7)(4\ell - 3)]}{[64\pi^2 a^2\eta^2\ell^2\omega^2 + K^2(7 - 4\ell)^2][576\pi^2 a^2\eta^2\ell^2\omega^2 + K^2(3 - 4\ell)^2]}. \tag{A11}$$

We also report the expression for the total work rate, Eq. (49):

$$\dot{W} = \frac{6\pi a_{12}\eta F_0^2\omega^2\big[a_1 a_2\cos(\Delta\phi)\big(a_1 a_2 K^2 - 4a_{12}^2(K^2 - 9\pi^2 a_1 a_2\eta^2\omega^2)\big] + a_{12}(a_1 + a_2)\big[4a_{12}^2(9\pi^2 a_1 a_2\eta^2\omega^2 + K^2) - a_1 a_2 K^2\big]\big)}{1296\pi^4 a_1^2 a_{12}^4 a_2^2\eta^4\omega^4 + 72\pi^2 a_{12}^2\eta^2 K^2\omega^2\big[a_1^2\big(2a_{12}^2 + a_2^2\big) + 2a_{12}^2 a_2^2\big] + K^4\big(a_1 a_2 - 4a_{12}^2\big)^2}. \tag{A12}$$

APPENDIX B: LIST OF SYMBOLS

TABLE I. List of symbols used in the text

a	radius of the three spheres
η	viscosity of the host fluid
$\mathbf{r_i}$	position vector of ith sphere (with $i = 1, 2, 3$)
$\mathbf{v_i}$	velocity vector of ith sphere (with $i = 1, 2, 3$)
u_i	relative velocity between particle i and particle $i + 1$ (with $i = 1, 2$)
$\mathbf{f_i}$	internal force vector
$\mathbf{f_i^R}$	external (thermal) noise force vector
$H_{ij}(\mathbf{r})$	mobility tensor
x_i	position along x axis of the ith sphere (with $i = 1, 2, 3$)
x_{cm}	position of the center of mass of the swimmer
L_i	distance between sphere i and sphere $i + 1$ (with $i = 1, 2$)
α	constant (with the dimensions of an inverse length) for the formula of average velocity, Eq. (7)
K	spring constant
l_i	length at rest of spring i joining sphere i and sphere $i + 1$ (with $i = 1, 2$)
ℓ	adimensional length at rest of springs, in the symmetric case $l_1 = l_2 = L = \ell a$
u_i	deformation of spring i joining sphere i and sphere $i + 1$ (with $i = 1, 2$)
$\mathbf{T}$, T_{ij}	mobility coefficient coupling x components of particles i and j
ζ	inverse of matrix $\mathbf{T}$
F_i	internal forces acting on particle i, components along x
F_i^{act}	internal forces acting on particle i of active origin, components along x
F_i^{pot}	internal forces acting on particle i of conservative origin (potential), components along x
F_i^R	noise forces acting on particle i of conservative origin (potential), components along x
$\underline{F}$, $\underline{F}^{\text{act}}$, $\underline{F}^{\text{pot}}$, $\underline{F}^R$	lists of total, active, potential and noise forces
v	average speed of the center of mass of the swimmer
ω	angular frequency (pulsation) of the active force (or of the displacement in the old models)
$\mathcal{T}$	period of the active force
ϕ_1, ϕ_2	phase of the active force on sphere i (or of its displacement in the old models)
F_0	amplitude of the active force ($F_0 = 10$ in all numerical results)
$\mathbf{D}$	diffusivity matrix of thermal noise
T	temperature
β	inverse thermal energy
$F_{\text{ito},i}$	Ito "force" on sphere i ($i = 1, 2, 3$) (dimensionally it is a velocity)
W, $\dot{W}$	work done by the active forces (total and average rate)
p, $p_{\max}$	thermodynamic precision and its maximum according to the TUR
D, D_0	coefficient of diffusion in the swimming direction and its bare value (thermal Einstein relation)
e_L, e_{TUR}	swimmer efficiencies with respect an effective hydrodynamic force and to the TUR bound
$\nu = \omega/2\pi$	forcing frequency
$v_0 = \omega a F_0^2/(L^2K^2)$	swimming velocity in the adiabatic limiti for small perturbation (linear theory)
$K_0 = F_0/a$	typical stiffness related
$\eta_0 = F_0/(6\pi v_0 a) = (KL)^2/(6\pi a^2 F_0 \omega)$	typical viscosity
$T_0 = F_0 * a$	typical thermal energy
$\nu_h = F_0/(6\pi\eta a^2)$	hydrodynamic frequency ($\omega_h = 2\pi\nu_h$)
$v_h = 2\pi\nu_h a F_0^2/(L^2K^2)$	swimming velocity associated to ω_h

[1] M. C. Marchetti, J.-F. Joanny, S. Ramaswamy, T. B. Liverpool, J. Prost, M. Rao, and R. A. Simha, Hydrodynamics of soft active matter, Rev. Mod. Phys. **85**, 1143 (2013).

[2] C. Bechinger, R. Di Leonardo, H. Löwen, C. Reichhardt, G. Volpe, and G. Volpe, Active particles in complex and crowded environments, Rev. Mod. Phys. **88**, 045006 (2016).

[3] Y. Fily and M. C. Marchetti, Athermal phase separation of self-propelled particles with no alignment, Phys. Rev. Lett. **108**, 235702 (2012).

[4] M. E. Cates and J. Tailleur, Motility-induced phase separation, Annu. Rev. Condens. Matter Phys. **6**, 219 (2015).

[5] A. Cavagna, I. Giardina, and T. S. Grigera, The physics of flocking: Correlation as a compass from experiments to theory, Phys. Rep. **728**, 1 (2018).

[6] J. Elgeti, R. G. Winkler, and G. Gompper, Physics of microswimmers-single particle motion and collective behavior: A review, Rep. Prog. Phys. **78**, 056601 (2015).

[7] I. H. Riedel-Kruse, A. Hilfinger, J. Howard, and F. Jülicher, How molecular motors shape the flagellar beat, HFSP Journal **1**, 192 (2007).

[8] C. Maggi, F. Saglimbeni, V. C. Sosa, R. Di Leonardo, B. Nath, and A. Puglisi, Thermodynamic limits of

sperm swimming precision, PRX Life **1**, 013003 (2023).
[9] K. Ishimoto, C. Moreau, and K. Yasuda, Odd elastohydrodynamics: Non-reciprocal living material in a viscous fluid, PRX Life **1**, 023002 (2023).
[10] E. M. Purcell, Life at low Reynolds number, Am. J. Phys. **45**, 3 (1977).
[11] E. Lauga, Life around the scallop theorem, Soft Matter **7**, 3060 (2011).
[12] G. S. Klindt and B. M. Friedrich, Flagellar swimmers oscillate between pusher- and puller-type swimming, Phys. Rev. E **92**, 063019 (2015).
[13] M. J. Lighthill, On the squirming motion of nearly spherical deformable bodies through liquids at very small Reynolds numbers, Commun. Pure Appl. Math. **5**, 109 (1952).
[14] A. Najafi and R. Golestanian, Simple swimmer at low Reynolds number: Three linked spheres, Phys. Rev. E **69**, 062901 (2004).
[15] R. Golestanian and A. Ajdari, Analytic results for the three-sphere swimmer at low Reynolds number, Phys. Rev. E **77**, 036308 (2008).
[16] J. Dunkel and I. M. Zaid, Noisy swimming at low Reynolds numbers, Phys. Rev. E **80**, 021903 (2009).
[17] M. Leoni, J. Kotar, B. Bassetti, P. Cicuta, and M. C. Lagomarsino, A basic swimmer at low Reynolds number, Soft Matter **5**, 472 (2009).
[18] R. Golestanian and A. Ajdari, Stochastic low Reynolds number swimmers, J. Phys.: Condens. Matter **21**, 204104 (2009).
[19] M. Chatzittofi, J. Agudo-Canalejo, and R. Golestanian, Entropy production and thermodynamic inference for stochastic microswimmers, Phys. Rev. Res. **6**, L022044 (2024).
[20] A. C. Barato and U. Seifert, Thermodynamic uncertainty relation for biomolecular processes, Phys. Rev. Lett. **114**, 158101 (2015).
[21] T. R. Gingrich, J. M. Horowitz, N. Perunov, and J. L. England, Dissipation bounds all steady-state current fluctuations, Phys. Rev. Lett. **116**, 120601 (2016).
[22] Y. Izumida, H. Kori, and U. Seifert, Energetics of synchronization in coupled oscillators rotating on circular trajectories, Phys. Rev. E **94**, 052221 (2016).
[23] S. Lee, C. Hyeon, and J. Jo, Thermodynamic uncertainty relation of interacting oscillators in synchrony, Phys. Rev. E **98**, 032119 (2018).
[24] Y. Hasegawa, Thermodynamics of collective enhancement of precision, Phys. Rev. E **98**, 032405 (2018).
[25] H. Hong, J. Jo, C. Hyeon, and H. Park, Thermodynamic cost of synchronizing a population of beating cilia, J. Stat. Mech.: Theory Exp. (2020) 074001.
[26] D. Zhang, Y. Cao, Q. Ouyang, and Y. Tu, The energy cost and optimal design for synchronization of coupled molecular oscillators, Nat. Phys. **16**, 95 (2020).
[27] M. P. Leighton and D. A. Sivak, Performance scaling and trade-offs for collective motor-driven transport, New J. Phys. **24**, 013009 (2022).
[28] B. U. Felderhof, The swimming of animalcules, Phys. Fluids **18**, 063101 (2006).
[29] J. Pande and A.-S. Smith, Forces and shapes as determinants of micro-swimming: effect on synchronisation and the utilisation of drag, Soft Matter **11**, 2364 (2015).
[30] A. Montino and A. DeSimone, Three-sphere low-reynolds-number swimmer with a passive elastic arm, Eur. Phys. J. E **38**, 42 (2015).
[31] G. Grosjean, M. Hubert, G. Lagubeau, and N. Vandewalle, Realization of the Najafi-Golestanian microswimmer, Phys. Rev. E **94**, 021101(R) (2016).
[32] F. Jülicher and J. Prost, Spontaneous oscillations of collective molecular motors, Phys. Rev. Lett. **78**, 4510 (1997).
[33] G. Costantini and A. Puglisi, Thermodynamic precision of a chain of motors: The difference between phase and noise correlation, J. Stat. Mech. (2024) 024003.
[34] R. Ma, G. S. Klindt, I. H. Riedel-Kruse, F. Jülicher, and B. M. Friedrich, Active phase and amplitude fluctuations of flagellar beating, Phys. Rev. Lett. **113**, 048101 (2014).
[35] G. J. Kynch, The slow motion of two or more spheres through a viscous fluid, J. Fluid Mech. **5**, 193 (1959).
[36] F. Box, E. Han, C. R. Tipton, and T. Mullin, On the motion of linked spheres in a Stokes flow, Exp. Fluids **58**, 29 (2017).
[37] K. Yasuda, Y. Hosaka, M. Kuroda, R. Okamoto, and S. Komura, Elastic three-sphere microswimmer in a viscous fluid, J. Phys. Soc. Jpn. **86**, 093801 (2017).
[38] C. W. Gardiner, *Handbook of Stochastic Methods* (Springer Berlin, 1985), Vol. 3.
[39] M. Doi and S. F. Edwards, *The Theory of Polymer Dynamics* (Oxford University, New York, 1988), Vol. 73.
[40] R. Kubo, The fluctuation-dissipation theorem, Rep. Prog. Phys. **29**, 255 (1966).
[41] U. M. B. Marconi, A. Puglisi, L. Rondoni, and A. Vulpiani, Fluctuation–dissipation: Response theory in statistical physics, Phys. Rep. **461**, 111 (2008).
[42] P. Mazur, On the motion and Brownian motion of *n* spheres in a viscous fluid, Physica A **110**, 128 (1982).
[43] A. W. C. Lau and T. C. Lubensky, State-dependent diffusion: Thermodynamic consistency and its path integral formulation, Phys. Rev. E **76**, 011123 (2007).
[44] Y. Hasegawa and T. Van Vu, Uncertainty relations in stochastic processes: An information inequality approach, Phys. Rev. E **99**, 062126 (2019).
[45] J. S. Lee, J.-M. Park, and H. Park, Universal form of thermodynamic uncertainty relation for Langevin dynamics, Phys. Rev. E **104**, L052102 (2021).
[46] A. Plati, A. Puglisi, and A. Sarracino, Thermodynamic bounds for diffusion in nonequilibrium systems with multiple timescales, Phys. Rev. E **107**, 044132 (2023).
[47] J. Pande, L. Merchant, T. Krüger, J. Harting, and A.-S. Smith, Setting the pace of microswimmers: When increasing viscosity speeds up self-propulsion, New J. Phys. **19**, 053024 (2017).
[48] G. Grosjean, M. Hubert, Y. Collard, S. Pillitteri, and N. Vandewalle, Surface swimmers, harnessing the interface to self-propel, Eur. Phys. J. E: Soft Matter Biol. Phys. **41**, 137 (2018).
[49] E. Lauga and T. R. Powers, The hydrodynamics of swimming microorganisms, Rep. Prog. Phys. **72**, 096601 (2009).
[50] S. Michelin and E. Lauga, Efficiency optimization and symmetry-breaking in a model of ciliary locomotion, Phys. Fluids **22**, 111901 (2010).
[51] B. Nasouri, A. Vilfan, and R. Golestanian, Efficiency limits of the three-sphere swimmer, Phys. Rev. Fluids **4**, 073101 (2019).
[52] S. E. Spagnolie, G. R. Moreno-Flores, D. Bartolo, and E. Lauga, Geometric capture and escape of a microswimmer colliding with an obstacle, Soft Matter **11**, 3396 (2015).

[53] T. Brotto, J.-B. Caussin, E. Lauga, and D. Bartolo, Hydrodynamics of confined active fluids, Phys. Rev. Lett. **110**, 038101 (2013).

[54] B. Zhang, P. Leishangthem, Y. Ding, and X. Xu, An effective and efficient model of the near-field hydrodynamic interactions for active suspensions of bacteria, Proc. Natl. Acad. Sci. USA **118**, e2100145118 (2021).

[55] B. M. Friedrich and F. Jülicher, Flagellar synchronization independent of hydrodynamic interactions, Phys. Rev. Lett. **109**, 138102 (2012).

[56] R. R. Bennett and R. Golestanian, Phase-dependent forcing and synchronization in the three-sphere model of chlamydomonas, New J. Phys. **15**, 075028 (2013).